Title: Functional architecture of the aging brain

Authors: Roni Setton[1*], Laetitia Mwilambwe-Tshilobo[1*], Manesh Girn[1], Amber W. Lockrow[1], Giulia Baracchini[1], Alexander J. Lowe[2], Benjamin N. Cassidy[3], Jian Li[4,5], Wen-Ming Luh[6], Danilo Bzdok[1,7,8,9,10] Richard M. Leahy[11], Tian Ge[12], Daniel S. Margulies[13], Bratislav Misic[1,8], Boris C. Bernhardt[1,8], W. Dale Stevens[14], Felipe De Brigard[15,16], Prantik Kundu[17], Gary R. Turner[14] and R. Nathan Spreng[1,8,18,19]

Affiliations:
[1] Montreal Neurological Institute, Department of Neurology and Neurosurgery, McGill University, Montreal, QC, Canada
[2] Institute of Neurology, University College London
[3] Department of Psychiatry, University of Toronto, Toronto, ON, Canada
[4]Athinoula A. Martinos Center for Biomedical Imaging, Department of Radiology, Massachusetts General Hospital, Charlestown, MA, USA
[5] Department of Neurology, Massachusetts General Hospital, Boston, MA, USA
[6] National Institutes of Health, National Institute on Aging, Baltimore, MD, USA
[7] Department of Biomedical Engineering, McGill University, Montreal, QC, Canada
[8] McConnell Brain Imaging Centre, McGill University, Montreal, QC, Canada
[9] School of Computer Science, McGill University, Montreal, QC, Canada
[10] Mila – Quebec Artificial Intelligence Institute, Montreal, QC, Canada
[11] Department of Electrical Engineering-Systems, University of Southern California, Los Angeles, CA, USA
[12] Psychiatric and Neurodevelopmental Genetics Unit, Center for Genomic Medicine, Massachusetts General Hospital, Boston, MA, USA
[13] Integrative Neuroscience and Cognition Center (UMR 8002), Centre National de la Recherche Scientifique (CNRS) and Université de Paris, Paris, France
[14] Department of Psychology, York University, Toronto, ON, Canada
[15] Department of Philosophy, Duke University, Durham, NC, USA
[16] Department of Psychology and Neuroscience, Durham, NC, USA
[17] Icahn School of Medicine at Mount Sinai, New York, NY, USA
[18] Departments of Psychiatry and Psychology, McGill University, Montreal, QC, Canada
[19] Douglas Mental Health University Institute, Verdun, QC, Canada

[*] Equal contribution

Correspondence:
R. Nathan Spreng
Montreal Neurological Institute
3801 University St.
Montréal, QC, H3A 2B4, Canada
p. 514-398-7268
f: 514-398-8248
e. nathan.spreng@gmail.com

Abstract

The intrinsic network architecture of the brain is continuously shaped by biological and behavioral factors from younger to older adulthood. Differences in functional networks can reveal how a lifetime of learning and lived experience can alter large-scale neurophysiological dynamics, offering a powerful lens into brain and cognitive aging. Quantifying these differences has been hampered by significant methodological challenges. Here, we use multi-echo fMRI and multi-echo ICA processing, individualized cortical parcellation methods, and multivariate (gradient and edge-level) functional connectivity analyses to provide a definitive account of the intrinsic functional architecture of the brain in older adulthood. Twenty minutes of resting-state multi-echo fMRI data were collected in younger (n=181) and older (n=120) adults. Dimensionality, the number of independent, non-noise BOLD components in the fMRI signal, was significantly reduced for older adults. Macroscale functional gradients were largely preserved. In contrast, edge-level functional connectivity was significantly altered. Within-network connections were weaker while connections between networks were stronger for older adults, and this connectivity pattern was associated with lower executive control functioning. Greater integration of sensory and motor regions with transmodal association cortices also emerged as a prominent feature of the aging connectome. These findings implicate network dedifferentiation, reflected here as reduced dimensionality within the BOLD signal and altered edge-level connectivity, as a global and putatively maladaptive feature of functional brain aging. However, greater coherence among specific networks may also signal adaptive functional reorganization in later life. By overcoming persistent and pervasive methodological challenges that have confounded previous research, the results provide a comprehensive account of the intrinsic functional architecture of the aging brain.

Keywords (5)

fMRI, connectivity, gradients, parcellation, network neuroscience, older adults, multi-echo

Spontaneous oscillations in brain activity provide the basis for characterizing large-scale functional networks (Biswal et al., 2010; Fox and Raichle, 2007; Yeo et al., 2011). This intrinsic functional network architecture is determined by both genetic factors and experience-dependent neuroplastic changes occurring across timescales, from moments to decades (Stevens and Spreng, 2014). Studying these networks in older adulthood can yield important insights into how a lifetime of learning and lived experience is instantiated in the aging brain. The intrinsic functional architecture of the brain, both in healthy aging and brain disease, was one of the earliest targets of inquiry examining low frequency blood-oxygen-level-dependent (BOLD) signal oscillations (Andrews-Hanna et al., 2007; Griecius et al., 2004), with nearly 1000 papers on the topic to date (National Library of Medicine). Unfortunately, isolating and reliably measuring changes to intrinsic functional brain networks from younger to older adulthood poses significant methodological challenges. Here we adopt a multi-faceted approach using novel, state-of-the-art fMRI data acquisition sequences, individualized functional cortical parcellations, and multivariate analytical approaches to provide a definitive depiction of age-differences in the intrinsic functional architecture of the human brain.

One of the most pervasive challenges confounding investigations of age differences in resting-state fMRI is the difficulty of separating neural from non-neural, or noise, components in BOLD signals. This is particularly problematic in cross-sectional studies of aging, where it can be difficult to attribute observed group differences to neural sources versus noise sources of non-interest. Here, to overcome this challenge, we adopted multi-echo fMRI (ME-fMRI) data acquisition with multi-echo independent components analysis (ME-ICA) preprocessing (Kundu et al., 2017). Innovations in ME-fMRI data acquisition protocols, combined with a TE-dependence model of BOLD signal denoising using ME-ICA, enables one to reliably differentiate BOLD from non-BOLD signal in fMRI data (Kundu et al., 2017). Importantly, ME-ICA processing eliminates the need for multiple confound regression, including the global signal (Spreng et al. 2019), while allowing for valid between-group comparisons of the full range of positive and negative resting state functional connectivity (RSFC) values. Previous work has demonstrated that dimensionality within the BOLD signal, or the number of independent functional BOLD components, declines from childhood to middle-adulthood and reflects dedifferentiation and integration of functional networks (Kundu et al., 2018). No previous report has examined differences in BOLD signal dimensionality from younger to older adulthood. However, as functional integration and reduced network differentiation are considered to be hallmarks of brain aging (Betzel et al., 2014; Madden et al., 2020; Malagurski et al., 2020; Stumme et al., 2020; Zonneveld et al., 2019), we predict that BOLD dimensionality, as a proxy for network dedifferentiation, will be significantly lower for older versus younger adults.

Valid comparison of RSFC between younger and older adults is also compromised when template registration is unable to account for the variation of the population under study (e.g., blurring of the ventricular boundaries due to inclusion of structurally intact younger and atrophic old adults; Buckner et al. 2004; Doucet et al., 2020). Yet variability in functional neuroanatomy cannot be aligned by anatomical registration alone (e.g., Haxby et al., 2011). In a study of lifespan RSFC differences, age-group specific parcellations showed higher internal validity relative to a standardized parcellation that was developed in younger adults and applied to older adults' data, and better-captured variability in task-evoked functional activation (Han et al., 2018). The relative sizes, locations, and spatial arrangements of cortical functional areas vary

considerably across individuals (Braga and Buckner, 2017; Chong et al., 2017; Gordon, et al. 2017; Kong et al., 2019; Kong et al., 2021; Laumann et al., 2015; Wang et al., 2015), highlighting the importance of individualized cortical parcellation methods. Here, we report the first application of functionally defined, individualized parcellations in the study of the aging brain. Deriving person-specific cortical parcellations can account for differences at the level of the individual, which will enable valid comparisons between age groups and, we predict, enhance our ability to detect reliable brain to behavior associations (Kong et al., 2021).

Finally, features of intrinsic brain network organization can be described at multiple spatial scales, from macroscale connectivity patterns to individual node-to-node connectivity strengths. Each approach conveys unique information about the spatial organization and coherence of RSFC networks and importantly, how they differ with age. Here we adopt both macroscale and edge-level analytic approaches to comprehensively characterize the intrinsic functional network architecture of the aging brain. We first conduct gradient analyses to characterize the macroscale, hierarchical organization of connectivity patterns across the cortex (Huntenburg et al., 2018; Margulies et al., 2016; Paquola et al., 2019; Vos de Wael et al., 2020). Connectivity gradients represent broad patterns of connectivity and thus can identify large-scale shifts in the functional architecture of the brain from younger to older adulthood (Bethlehem et al., 2020). Second, we adopt partial least squares (PLS, Krishnan et al., 2011; McIntosh and Misic, 2013) to investigate edge-level functional connectivity differences in aging. This represents an important advance as commonly used seed or component (e.g. ICA) based approaches to measure connectivity are sensitive to decisions on statistical thresholding or component labeling. PLS analyzes the full edge-level connectivity matrix in a single statistical step, eliminating the need for additional thresholding within an *a priori* defined network parcellation scheme. We predict that this matrix-wise analytical approach will reveal additional features of the aging RSFC connectome which heretofore may have been masked by idiosyncratic analysis choices in previous studies. .

In adopting this multi-faceted approach, from acquisition to analytics, the present study aims to provide the most precise and comprehensive account of intrinsic functional brain differences in older adulthood to date. Specifically, we implement three key methodological advances: ME-fMRI acquisition and ME-ICA processing, individualized network node parcellation, and multivariate (macroscale and edge-level) functional connectivity analyses. Leveraging these approaches, we conducted five analyses to characterize the functional architecture of the aging brain. First, we contrasted BOLD dimensionality, derived from ME-ICA, in younger versus older adults. Second, we identified age-related macroscale architectural changes through analysis of RSFC gradients. Third, we quantified age differences in the functional connectome between younger and older adults. Fourth, we identified functional relationships among BOLD dimensionality, cortical gradients, and whole-brain RSFC. Finally, we determined associations between these measures of intrinsic functional connectivity and cognition.

Materials and Methods

Participants

Participants were 181 younger (M_{age}=22.59y, *SD*=3.27; 57% female) and 120 older (M_{age}=68.63y, *SD*=6.44; 54% female) healthy adults from Ithaca, New York, and Toronto, Canada (Table 1), rendering a total sample size of 301. Participants were screened to rule out individuals with a history of neurological or other medical illness known to impact cognition, acute or chronic psychiatric illness, those undergoing current or recent treatment with psychotropic medication, and those having experienced significant changes to health status within three months of the eligibility interview. Younger and older participants were screened for depressive symptoms using the Beck Depression Inventory (Beck et al., 1996) or the Geriatric Depression Scale (Yesavage et al., 1982), respectively. Two older adults were excluded due to a rating of "moderate depression". Older adults were additionally administered the Mini-Mental State Examination (MMSE; Folstein et al., 1975) to rule out mild cognitive impairment or sub-clinical dementia. Participants with MMSE scores below 27/30 were excluded if fluid cognition scores (Gershon et al., 2013) also fell below an age-adjusted national percentile of 25%. All participants were right-handed with normal or corrected-to-normal vision. Procedures were administered in compliance with the Institutional Review Board at Cornell University and the Research Ethics Board at York University.

Cognitive Assessment

283 of 301 individuals (163/181 younger adults, 120/120 older adults) underwent extensive cognitive assessment over three to four days prior to brain scanning. Index scores were created for cognitive domains of episodic memory, semantic memory, executive function, and processing speed (descriptives in Table 1). Episodic memory tasks included Verbal Paired Associates from the Wechsler Memory Scale-IV (Wechsler, 2009), the Associative Recall Paradigm (Brainerd et al., 2014), and NIH Cognition Toolbox Rey Auditory Verbal Learning and Picture Sequence Memory Tests (Gershon et al., 2013). Semantic memory tasks included Shipley-2 Vocabulary (Shipley et al., 2009), and NIH Cognition Toolbox Picture Vocabulary and Oral Reading Recognition Tests (Gershon et al., 2013). Executive function comprised the Trail Making Test (B-A; Reitan, 1958), the Reading Span Task (Daneman & Carpenter, 1980), NIH Cognition Toolbox Flanker Inhibitory Control and Attention task, Dimensional Change Card Sort, and List Sort Working Memory Tests (Gershon et al., 2013). Processing speed was tested with the Symbol Digit Modalities Test, Oral (Smith, 1982).

All data were z-scored. Index scores represent the average z-score (reversed where relevant) for all measures included within a cognitive domain. Across the four domains, higher scores represent better performance. Brain-behavior product-moment correlations were conducted at an alpha level of .05 with 83% confidence intervals (Austin & Hux, 2002) and Bonferroni adjustment for multiple comparison of $p<.013$ for four index score tests.

Table 1

Sample Demographics

	Younger Adults	Older Adults
N		
Cornell	154 (86 female)	84 (47 female)
York	27 (17 female)	36 (18 female)
Age (years)		
Range	18-34	60-89
M	22.6	68.6
SD	3.3	6.4
Education (years)*		
Range	12-24	12-24
M	15.2	17.2
SD	1.9	2.9
Episodic Memory*		
Range	-1.75-1.59	-1.99-0.70
M	0.52	-0.71
SD	0.53	0.66
Semantic Memory*		
Range	-2.78-1.39	-1.29-1.91
M	-0.35	0.48
SD	0.77	0.71
Executive Function*		
Range	-1.15-1.80	-2.03-0.76
M	0.36	-0.48
SD	0.56	0.53
Processing Speed*		
Range	-2.26-3.05	-2.40-.050
M	0.57	-0.78
SD	0.86	0.56

Table 1 Note: Episodic Memory, Semantic Memory, and Executive Function are index scores. Processing Speed is a z-score on Symbol Digit Modalities Task, Oral. * significant group differences.

Neuroimaging

Image Acquisition

Imaging data were acquired on a 3T GE750 Discovery series MRI scanner with a 32-channel head coil at the Cornell Magnetic Resonance Imaging Facility or on a 3T Siemens Tim Trio MRI scanner with a 32-channel head coil at the York University Neuroimaging Center in Toronto. Scanning protocols were closely matched across sites. Anatomical scans at Cornell were acquired using a T1-weighted volumetric magnetization prepared rapid gradient echo sequence (TR=2530ms; TE=3.4ms; 7° flip angle; 1mm isotropic voxels, 176 slices, 5m25s) with 2x acceleration with sensitivity encoding. At York, anatomical scans were acquired using a T1-weighted volumetric magnetization prepared rapid gradient echo sequence (TR=1900ms; TE=2.52ms; 9° flip angle; 1mm isotropic voxels, 192 slices, 4m26s) with 2x acceleration and generalized auto calibrating partially parallel acquisition (GRAPPA) encoding at an iPAT acceleration factor of 2. Two 10m06s resting-state runs were acquired using a multi-echo (ME) EPI sequence at Cornell University (TR=3000ms; TE_1=13.7ms, TE_2=30ms, TE_3=47ms; 83° flip angle; matrix size=72x72; field of view (FOV)=210mm; 46 axial slices; 3mm isotropic voxels; 204 volumes, 2.5x acceleration with sensitivity encoding) and York University (TR=3000ms; TE_1=14ms, TE_2=29.96ms, TE_3=45.92ms; 83° flip angle; matrix size=64x64; FOV=216mm; 43 axial slices; 3.4x3.4x3mm voxels; 200 volumes, 3x acceleration and GRAPPA encoding). Participants were instructed to stay awake and lie still with their eyes open, breathing and blinking normally in the darkened scanner bay.

Image Processing

Anatomical images were skull stripped using the default parameters in FSL BET (Smith, 2002). Brain-extracted anatomical and functional images were submitted to ME-ICA (version 3.2 beta; https://github.com/ME-ICA/me-ica; Kundu et al., 2011; Kundu et al., 2013). ME-ICA relies on the TE-dependence model of BOLD signal to determine T2* in every voxel and separates BOLD signal from non-BOLD sources of noise. Prior to TE-dependent denoising, time series data were minimally preprocessed: the first 4 volumes were discarded, matrices were computed for de-obliquing, motion correction, and anatomical-functional coregistration, and volumes were brought into spatial alignment across TEs. The T2* maps were then used for anatomical-functional coregistration. Gray matter and cerebrospinal fluid compartments are more precisely delineated by the T2* map than by raw EPI images (Speck et al., 2001; Kundu et al., 2017), which is an important consideration in aging research where these boundaries are often blurred by enlarged ventricles and greater subarachnoid space. Volumes were then optimally combined across TEs and denoised.

Image quality assessment was performed on the denoised time series in native space to identify and exclude participants with unsuccessful coregistration, residual noise (in-scanner motion >3 mm coupled with denoised time series showing DVARS >1, Power et al., 2012), poor temporal signal to noise ratio < 50, or fewer than 10 retained BOLD-like components (see Supplementary Figure 1 for the group temporal signal to noise map).

The denoised BOLD component coefficient sets in native space, optimized for functional connectivity analyses (Kundu et al., 2013), were used in subsequent steps. We refer to these as multi-echo functional connectivity (MEFC) data. Additional measures were taken to account for variation in the number of independent components from ME-ICA once connectivity matrices

were estimated, as detailed below. MEFC neuroimages were mapped to a common cortical surface for each participant using FreeSurfer v6.0.1 (Fischl et al., 2012). To maximize alignment between intensity gradients of structural and functional data (Greve & Fischl, 2009), MEFC data were first linearly registered to the T1-weighted image by run. The inverse of this registration was used to project the T1-weighted image to native space and resample the MEFC data onto a cortical surface (fsaverage5) with trilinear volume-to-surface interpolation. Once on the surface, runs were concatenated and MEFC data at each vertex were normalized to zero mean and unit variance.

Individualized Parcellation. We generated participant-specific functional parcellations to examine individual differences in functional brain network organization using the Group Prior Individual Parcellation (GPIP; Chong et al., 2017). This approach enables a more accurate estimation of participant-specific individual functional areas (Chong et al., 2017) and is more sensitive to detecting RSFC associations with behavior (Kong et al., 2019; Mwilambwe-Tshilobo et al., 2019). The main advantage of this approach is that the correspondence among parcel labels is preserved across participants, while the parcel boundaries are allowed to shift based on the individual-specific functional network organization of each participant—thus providing a similar connectivity pattern that is shared across the population. Starting from an initial pre-defined group parcellation atlas, GPIP first refines each individual's parcel boundaries relative to their resting-state fMRI data. Next, the concentration (inverse covariance/partial correlation) matrices from all subjects are jointly estimated using a group sparsity constraint. GPIP iterates between these two steps to continuously update the parcel labels until convergence. Compared to other group-based parcellation approaches, GPIP has shown to improve the homogeneity of the BOLD signal within parcels and the delineation between regions of functional specialization (Chong et al., 2017).

We extracted MEFC data from each vertex and applied the above parcellation across the entire cohort of 301 participants at resolutions of 200 and 400 parcels. For each resolution, MEFC data were initialized to a group parcellation atlas developed by Schaefer et al. (2018). The two-step iterative process was repeated 20 times to produce a final parcellation representing the optimal partition with respect to the entire cortical surface. We calculated homogeneity by taking the average correlation coefficient of all pairs of vertices in a given parcel and then averaging across all parcels. This was repeated at each repetition to observe the incremental change in homogeneity as the iterative parcellation proceeded. Homogeneity was calculated first at the participant level and then averaged across the entire cohort for a group estimate. For a subset of participants, some parcels from the final partition merged into the medial wall (where no data existed) or into parcels belonging to the contralateral hemisphere. Because partitions likely reflect participant-specific neurobiological variations in functional organization, parcels assigned to the contralateral hemisphere were allowed to retain their original group atlas label. With the 400-parcel resolution, parcels merging with the medial wall occurred in 69 older adults and 35 younger adults, averaging 2-3 parcels in these participants; parcels migrating to the contralateral hemisphere occurred in 62 older adults and 24 younger adults, averaging 2-3 parcels. With the 200-parcel resolution, parcels merging with the medial wall occurred in 18 older adults and 10 younger adults, averaging 1 parcel in these participants. No parcels migrated to the contralateral hemisphere at this resolution.

Functional Connectivity Matrix. A connectivity matrix was constructed for each participant according to their individualized parcel solution. We extracted and spatially averaged the resulting MEFC data from each parcel and computed the product-moment correlation

between each pair, resulting in a $n_{parcels} \times n_{parcels}$ functional connectivity matrix (Ge, Holmes, Buckner, Smoller, & Sabuncu, 2017). In this approach, RSFC was calculated as the correlation of the ICA coefficients across parcels, rather than a correlation across BOLD signal time-series, as is typically done (see Kundu et al., 2013). The canonical Fisher's r-to-z transformation was then applied to normalize the distribution of correlation values and account for variation in MEFC data degrees of freedom, or the number of de-noised ICA coefficients, across individuals (Kundu et al., 2013):

$$Z = \text{arctanh}(R) \cdot \sqrt{df - 3}$$

where R is the product-moment correlation value and *df* refers to the number of denoised ICA coefficients. Computing functional connectivity with approximately independent component coefficients rendered global signal regression unnecessary (Spreng et al., 2019). Critically, ME-ICA effectively removes distance-dependent RSFC motion confounds from fMRI data (Power et al., 2018).

Analysis

BOLD Dimensionality

A unique advantage of ME-fMRI and the ME-ICA processing framework is that BOLD- and non-BOLD-like signals can be separated into independent components. A novel metric of "BOLD dimensionality," the number of BOLD components identified in the ME-fMRI time series, may then be examined (e.g. Kundu et al., 2018). We assessed the test-retest reliability of BOLD dimensionality across two runs of data. Total BOLD dimensionality was then compared between groups with an independent samples *t*-test. To observe the trajectory of BOLD dimensionality with increasing age across the lifespan, BOLD dimensionality data from an independent developmental sample (N = 51, 10 female; M_{age}=21.9 years; age range, 8.3 – 46.2 years; see Kundu et al., 2018 for details) were pooled with the current data. To render the samples comparable and account for differences in acquisition across datasets, BOLD dimensionality was scaled by the number of timepoints acquired. The relationship between age and BOLD dimensionality was then fit to a power law function (see Supplementary Figure 2 for unscaled version).

Gradients & Manifold Eccentricity

Cortical gradients were computed using functions from the BrainSpace toolbox (https://github.com/MICA-MNI/BrainSpace; Vos de Wael et al., 2020), as implemented in MATLAB. For each participant, the 400 x 400 GPIP functional connectivity matrix was thresholded row-wise to the upper 10% of connections to retain only the strongest positive connections (Hong et al., 2019; Margulies et al., 2016). Cosine similarity was computed on the sparse matrix to input to the diffusion map embedding algorithm employed below, generating a matrix that captures similarity in whole-brain connectivity patterns between vertices (Hong et al., 2019; Margulies et al., 2016).

We then applied diffusion map embedding, a non-linear dimensionality manifold learning technique from the family of graph Laplacians (Coifman et al., 2005), to identify gradient components at the individual participant level. Each gradient represents a low-dimensional embedding estimated from a high-dimensional similarity matrix. In the embedding space,

vertices that feature greater similarity in their whole-brain functional connectivity patterns appear closer together, whereas vertices that are dissimilar are farther apart. Each embedding axis can thus be interpreted as an axis of variance based on connectivity pattern similarity/dissimilarity. Euclidean distance in the embedded space is equivalent to the diffusion distance between probability distributions centered at those points, each of which is equivalent to a *difference in gradient* score. The algorithm is controlled by a single parameter α, which controls the influence of density of sampling points on the manifold with $\alpha = 0.5$ (Margulies et al, 2016). This differentiates diffusion map embedding from Laplacian eigenmaps, and allows the inclusion of both global and local relationships in the estimation of the embedded space. An iterative Procrustes rotation was performed to align participant-specific gradient components to a Young-Old group average template and enable group comparisons. Group contrasts were conducted using surface-based linear models, as implemented in Surfstat (Worsley et al., 2009; http://www. math.mcgill.ca/keith/surfstat/).

We calculated a metric of manifold eccentricity to quantify the diffusivity of vertices in gradient space. Following Bethlehem et al. (2020) and Park et al. (2020), we summed the squared Euclidean distance of each vertex from the whole-brain median in a 2-dimensional gradient space for each participant. Mean manifold eccentricity was then compared across age groups. Statistical significance was determined with spin-test permutation testing, which overcomes biases in the test statistic due to the spatial autocorrelation inherent to BOLD data (Alexander-Bloch et al., 2018).

Edge-level Connectomics

Inter-regional functional connectivity group differences were determined with partial least squares (PLS). PLS is a multivariate method that determines the association between two sets of variables by identifying linear combinations of variables in both sets that maximally covary together (McIntosh and Lobaugh, 2004; McIntosh and Misic, 2013). In our analyses, one set of variables was individual RSFC matrices, while the other set represented group assignment or individual difference metrics.

Functional connectivity was assessed at the whole-brain level using the Schaefer atlas (Schaefer et al., 2018; Yeo et al., 2011; 400 x 400 matrix; 200 x 200 matrix as supplementary analysis, Supplementary Figure 3). Motivated by prior work (e.g., Grady et al., 2016; Sullivan et al., 2019; Spreng et al., 2016), we also examined RSFC among sub-networks of the default, frontoparietal control, and dorsal attention networks. For the sub-network analysis, we first reassigned each of the 400 parcels to the corresponding network of the Yeo 17-network solution following the mapping based on Schaefer et al. (2018). Next, we created a matrix for the pairwise connections between the following 8 sub-networks: dorsal attention (DAN-A, DAN-B), frontoparietal control (CONT-A, CONT-B, CONT-C), and default (DN-A, DN-B, DN-C) resulting in a 192x192 parcel matrix. The full 17-network characterization of the 400x400 parcel results, along with the 17-network and sub-network characterizations of the 200x200 matrix, can be found in Supplementary Figures 4, 5, and 7. At each level, a data matrix **X** was created using all participants' parcellated functional connectivity matrices. The **X** matrix was organized such that each row corresponded to an observation (each participant, nested in age groups), and the cells in each column corresponded to the unique connections from each participant's connectivity matrix (the lower triangle of the matrix). The column means within each group were calculated, and the data in **X** were mean-centered. The mean-centered data were then submitted to singular value decomposition (SVD) to provide mutually orthogonal latent variables. Each latent variable

represents a specific relationship (e.g. RSFC x Group) and consists of three elements: (1) a left singular vector consisting of the weighted connectivity pattern that optimally expresses the covariance, (2) a right singular vector, which represents the weights of the study design variables and can be interpreted as data-driven contrast weights between groups, and (3) a scalar singular value, which represents the covariance strength between the design variables (Group) and RSFC accounted for by each latent variable. Brain connectivity scores were calculated by taking the dot product of the left singular vector and each participant's RSFC matrix. A brain connectivity score, therefore, represents a single measure of the degree to which a participant expresses the connectivity pattern captured by a given latent variable.

Behavioral PLS was used to further investigate patterns of RSFC related to individual differences of interest: BOLD dimensionality and gradient manifold eccentricity (see above for details). In this variation of PLS, two matrices, **X** and **Y**, were computed. As above, **X** contained each participant's functional connections, while each column of **Y** contained the individual difference measure of interest for each participant organized by group membership. The **X** and **Y** matrices were mean centered, normalized, and submitted to SVD. The cross-correlation matrix **X**'**Y** produced latent variables identifying the similarities and differences between age groups and their associations between RSFC and individual difference measures.

All PLS latent variables were statistically evaluated using permutation testing. Rows of **X** were randomly reordered and subjected to SVD iteratively, as described above. This was done 1,000 times, creating a distribution of singular values under the null hypothesis of no existing relationships between X and Y for the corresponding PLS analysis, that there is no group difference in 1) whole-brain (or sub-network) RSFC or 2) brain-behavior correlations. A *p*-value was computed for each latent variable as the proportion of permuted singular values greater than or equal to the original singular value. Critically, permutation tests involve the entire multivariate pattern and are performed in a single analytic step, so correction for multiple comparisons is not required (McIntosh and Lobaugh, 2004).

Bootstrap resampling was used to estimate the reliability of weights for each RSFC edge. Participants were randomly resampled (rows in **X**) with replacement while respecting group membership. The matrix was subjected to SVD and the process was repeated 1,000 times, generating a sampling distribution for the weights in the singular vectors. To identify individual connections that made a statistically significant contribution to the overall connectivity pattern, we calculated the ratio between each weight in the singular vector and its bootstrap-estimated standard error. Bootstrap ratios are equivalent to z-scores if the bootstrap distribution is approximately unit normal (Efron and Tibshirani, 1986). Bootstrap ratios were, therefore, thresholded at values of ±1.96, corresponding to the 95% CI.

Network-Level Contributions

PLS analyses identified inter-regional connectivity patterns that differed by group and/or covaried with individual difference metrics. For each of these analyses, network-level effects were also examined. To quantify the network-level contributions to the PLS-derived functional connectivity pattern, two separate weighted adjacency matrices were constructed from positive and negative RSFC weights. For both matrices, nodes represent parcels defined by the individual parcellation, while edges correspond to the thresholded bootstrap ratio of each pairwise connection. Network-level functional connectivity contributions were quantified by assigning each parcel according to the network assignment reported by Yeo et al. (2011), and taking the average of all connection weights in a given network, thereby generating a 7 x 7 matrix (17 x 17

matrix for the 17-network solution; and an 8 x 8 matrix when examining interactivity for the default, frontoparietal control, and dorsal attention sub-networks). The significance of mean within- and between- network connectivity was computed by permutation testing. During each permutation, network labels for each node were randomly reordered and the mean within- and between- network connectivity were recalculated. This process was repeated 1000 times to generate an empirical null sampling distribution that indicates no relationship between network assignment and connectivity pattern (Shafiei et al., 2019). The significance of the pairwise connections of the original network matrix was determined by estimating the proportion of times the value of the sampling distribution was greater than or equal to the original value.

Network Visualization

Spring-embedded plots were rendered from group average matrices of RSFC data using Pajek software (Mrvar & Batagelj, 2016). Sparse matrices containing the top 5% of positive connections (unless otherwise noted) were created and fed into Pajek. A partition was assigned based on the Yeo 7 or 17 network solution (Yeo et al., 2011) to optimize community (i.e., network) structure for visualization.

Results

BOLD Dimensionality

BOLD dimensionality was stable across resting-state fMRI runs ($r(299) = .79$, $p < .001$, [.75, .83]; Figure 1A). Younger adults showed greater BOLD dimensionality than older adults ($t(299)=15.38$, $p < .001$; Cohen's $d= 1.81$; Figure 1B). In the context of lifespan development, which included the additional developmental sample aged 8-46 (Kundu et al., 2018), a power function provided a suitable fit between age and BOLD dimensionality ($R^2=.547$; Figure 1C).

Figure 1

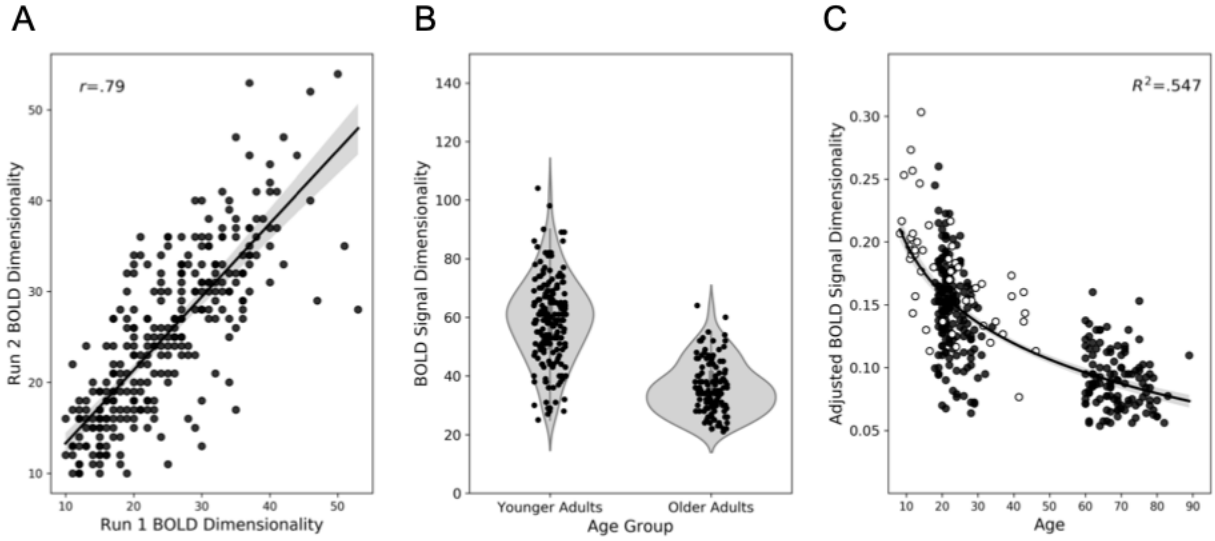

Figure 1 Caption: BOLD signal dimensionality (A) High test-retest reliability across 2 ME-fMRI runs. (B) Violin plots show distributions of total BOLD signal components for both runs in younger and older adults. (C) The scatter plot shows BOLD signal dimensionality by age with a power distribution and 95% confidence intervals overlaid. Points in white were contributed by Kundu and colleagues (2018). Adjusted BOLD signal dimensionality = Total number of accepted BOLD components / number of time points acquired.

Gradients & Manifold Eccentricity

We next characterized gradients of functional connectivity in younger and older adults (e.g., Girn et al., 2020; Hong et al., 2019; Margulies et al., 2016). In both groups, the principal gradient spanned from unimodal regions to transmodal regions (Figure 2A). A whole-brain age group comparison revealed higher gradient values within bilateral superior parietal lobule in older adults (FWE $p < .05$; cluster defining threshold $p < .01$; Figure 2A). Here, higher gradient values represent greater functional connectivity similarity with transmodal regions as opposed to unimodal regions. In older adults, the superior parietal lobule is more closely affiliated with heteromodal cortex, including the default network, than in younger adults. The second gradient of cortical connectivity displayed an axis of functional connectivity pattern similarity spanning visual cortex on one end to somatomotor and auditory cortices on the other (Figure 2B). Whole-brain group comparisons revealed no significant differences in the second gradient.

We rendered principal-second gradient manifold scatterplots in a 2D gradient embedding space in younger and older adults (Figure 2C). Older adults showed more diffuse and dedifferentiated vertices. We quantified this diffusivity by calculating manifold eccentricity –the sum of Euclidean distance across all vertices from the median– for each participant and compared across groups. Results revealed significantly greater manifold eccentricity in older adults ($t(299) = -10.74$, $p_{SPIN} < 0.01$, Cohen's $d = 1.26$).

Figure 2

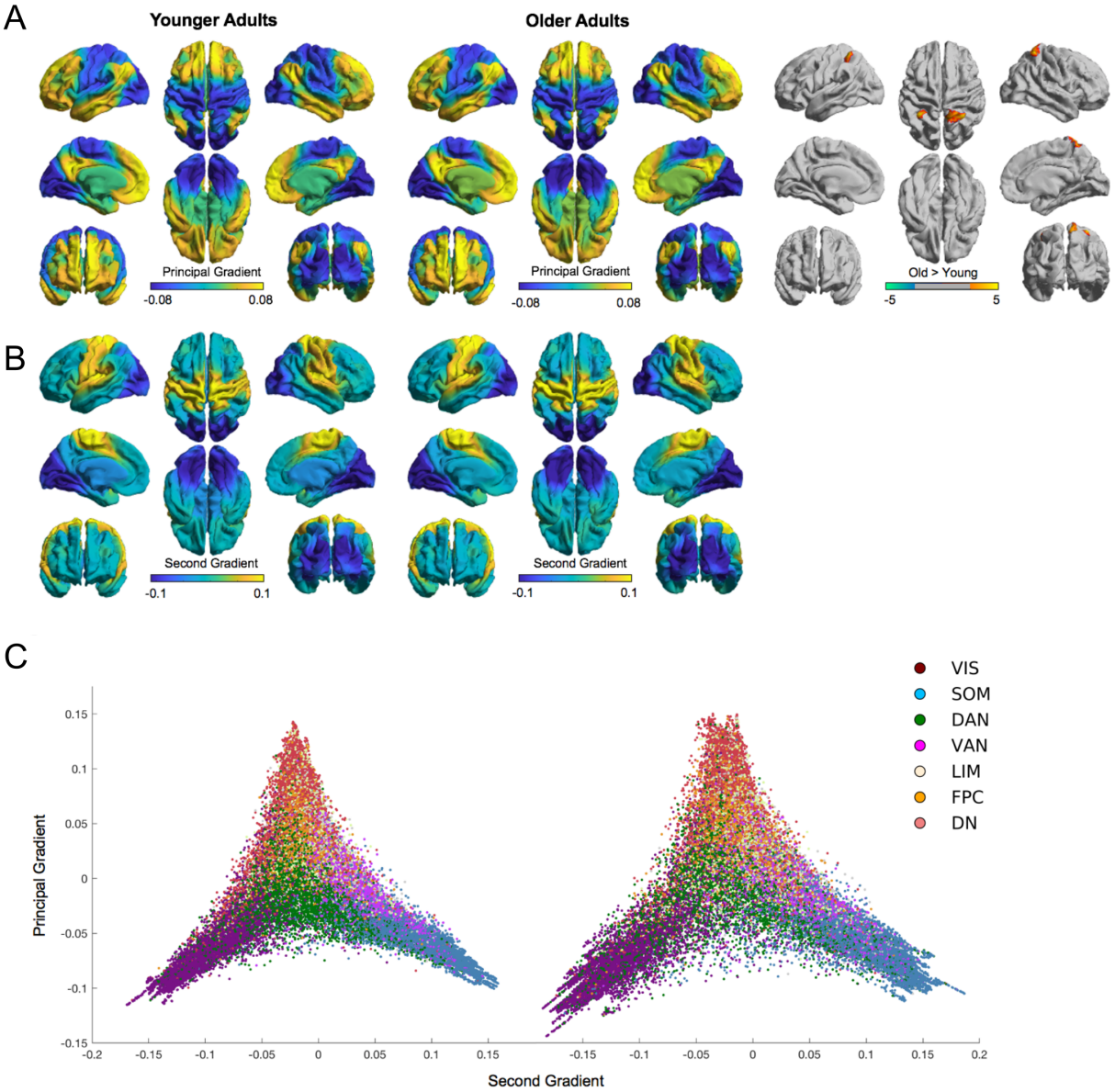

Figure 2 Caption: Gradients of cortical connectivity in younger and older adults. (A) The mean principal gradient for younger (left) and older (center) adults, representing an axis of functional connectivity similarity variance that ranged lowest to highest from unimodal to transmodal cortex. Older adults > younger adults contrast revealing statistically significant clusters at FWE $p < 0.05$, cluster defining threshold $p < 0.01$ (right). (B) The mean second gradient for younger (left) and older (right) adults, representing an axis of functional connectivity similarity variance that ranged lowest to highest from visual to somatomotor cortex. No group differences were observed for the second gradient. (C) Scatterplots representing the principal-second gradient manifold for younger (left) and older (right) adults. Scatter plot colors indicate functional network as per the 7-network parcellation scheme by Yeo et al. (2011). VIS = visual, SOM= somatomotor, DAN= dorsal attention, VAN = ventral attention, LIM = limbic, FPC= frontoparietal, DN= default.

Connectomics

We next examined whole-brain interregional functional connectivity differences between younger and older adults. Group mean connectivity matrices are in Figure 3A-B. A simple visual comparison makes clear that a number of low-weighted negative connections in younger adults shift to low-weighted positive connections in older adults (e.g., connectivity between the visual and other systems). Qualitative differences in the top 5% of positive connections between groups can be observed with a spring-embedded layout arranged by their network membership (Figure 3C-D). Visual comparison of these plots underscores the pattern of network dedifferentiation observed in older adults.

Age-related differences in the 79800 interregional connections (i.e., the lower triangle of the 400x400 functional connectivity matrix) were quantitatively assessed with PLS. A significant latent variable (permuted p = 0.0001) revealed a pattern of age differences in RSFC, with increases and decreases observed across the connectome (Figure 3E). Network contribution analysis of within- and between- network means revealed significant age effects. Older adults demonstrated lower within-network connectivity across all 7 systems, and lower connectivity between limbic, frontoparietal control and default networks (Figure 3F). Older adults showed greater between-network connectivity across systems for the visual and somatomotor networks (Figure 3G). The overall pattern of age-related differences was similar when examined with a 200 parcellation scheme (Supplementary Figure 3).

Figure 3.

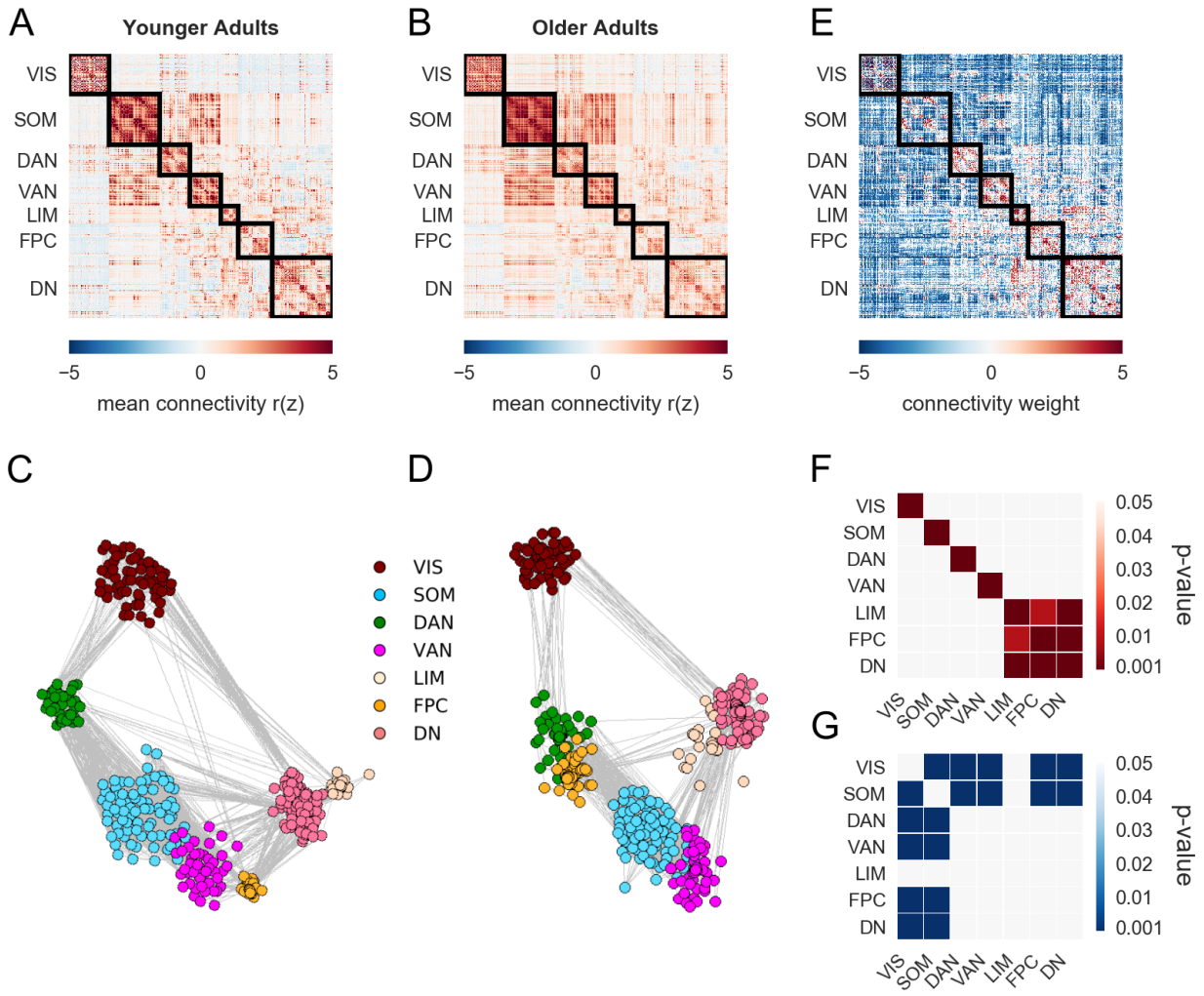

Figure 3 Caption: Functional connectomics in younger and older adults. Mean RSFC for the 400-parcellated MEFC data in (A) younger and (B) older adults. Spring-embedded plots with a 7-network solution (5% edge density) of the mean correlation matrices for (C) younger and (D) older adults. (E) Multivariate PLS analysis was used to identify age-related differences in RSFC between younger and older adults. Red color indicates significantly greater RSFC in younger adults, and blue color indicates significantly greater RSFC in older adults. (F-G) Network contributions reflecting differences in large-scale distributed networks. (F) Greater within- and between- network connectivity in younger adults. (G) Greater within- and between- network connectivity in older adults. The mean positive (F) and negative (G) bootstrap ratios within and between networks are expressed as a p-value for each z-score relative to a permuted null model. Higher z-scores indicate greater connectivity than predicted by the null distribution. VIS = visual, SOM= somatomotor, DAN= dorsal attention, VAN = ventral attention, LIM = limbic, FPC= frontoparietal, DN= default.

Connectomics of BOLD Dimensionality & Manifold Eccentricity

BOLD dimensionality and manifold eccentricity both demonstrated significant age-group differences. We conducted post-hoc product-moment correlations between them to determine the relationship between BOLD dimensionality and manifold eccentricity separately within each age group. Negative correlations were observed in both younger ($r(179)= -.575$, $p < .001$, [-.64, -.50]) and older adults ($r(118)= -.255$, $p < .005$, [-.37, -.13]), such that higher BOLD dimensionality was related to less diffuse, more compact vertices in the manifold (Figure 4A). In computing a partial correlation controlling for age, the relationship remained when performed on the full sample ($pr(299)= -.391$, $p < .001$, [-.48, -.29]). Non-overlapping 83% confidence intervals (Austin & Hux, 2002) indicated a significantly stronger correlation in younger adults.

We next examined how BOLD dimensionality and manifold eccentricity related to functional connectivity in a behavioral PLS analysis. Although a canonical Fisher's r-to-z transform was applied to statistically account for varying degrees of freedom across participants (i.e., number of BOLD components), we re-introduced BOLD dimensionality as an individual difference measure given its shift over the lifespan (Figure 1). In addition, treating manifold eccentricity as a behavioral measure let us explore the functional connectivity underlying the manifold expansion observed in our large-scale gradient results (Figure 2C). Thus, a PLS was computed which included both metrics as one variable set and interregional RSFC as the other. This enabled an examination of each metrics' shared and diverging effects on pairwise connections in younger and older adults. See Supplementary Figure 6 for same analysis with the 200-region parcellation.

PLS analysis identified three significant latent variables. The first latent variable expressed the inverse correlation between BOLD dimensionality and manifold eccentricity by dissociating connectivity related to each metric across groups (permuted $p < 0.0001$; 51.64% covariance explained; Figure 4B). The pattern of functional connectivity reproduced the principal gradient's poles of sensory-motor to transmodal networks. Higher BOLD dimensionality and lower manifold eccentricity was associated with higher connectivity along the diagonal and between the default, frontoparietal, and limbic networks (younger adults: BOLD dimensionality $r = 0.86$, manifold eccentricity $r = -0.68$; older adults: BOLD dimensionality $r = 0.66$, manifold eccentricity $r = -0.47$), a pattern more strongly observed in younger adults. Lower BOLD dimensionality and greater manifold eccentricity were associated with higher within- and between- network connectivity of the visual and somatomotor networks.

In the second latent variable, a shared pattern of connectivity emerged among BOLD dimensionality and manifold eccentricity in older adults that covaried with manifold eccentricity in younger adults (permuted $p < 0.0001$; 29.11% covariance explained; younger adults: BOLD dimensionality $r = -.03$, manifold eccentricity $r = -0.37$; older adults: BOLD dimensionality $r = -0.58$, manifold eccentricity $r = -0.40$; Figure 4C). BOLD dimensionality in younger adults did not contribute to this pattern. Higher manifold eccentricity in both groups and higher BOLD dimensionality in older adults was associated with greater inter-regional connectivity within all networks—although this pattern was concentrated within and between the somatomotor network. Lower manifold eccentricity in both groups and lower BOLD dimensionality in older adults was associated with greater between-network visual connectivity, along with greater default-ventral attention, default-frontoparietal control, and frontoparietal control-limbic between-network connectivity.

The third latent variable identified a pattern of connectivity in the younger adults only which covaried with BOLD dimensionality and manifold eccentricity (permuted p = 0.001; 4.52% covariance explained; younger adults: BOLD dimensionality r = -0.39, manifold eccentricity r = -0.41; older adults: BOLD dimensionality r = 0.05, manifold eccentricity r = 0.02; Figure 4D). BOLD dimensionality and manifold eccentricity showed a steep negative correlation in younger adults (Figure 4A). While the pattern explained a small portion of the overall variance it manifested in a more interconnected visual network, and a pattern of lower between-network connectivity of the limbic, frontoparietal control and default networks.

Figure 4

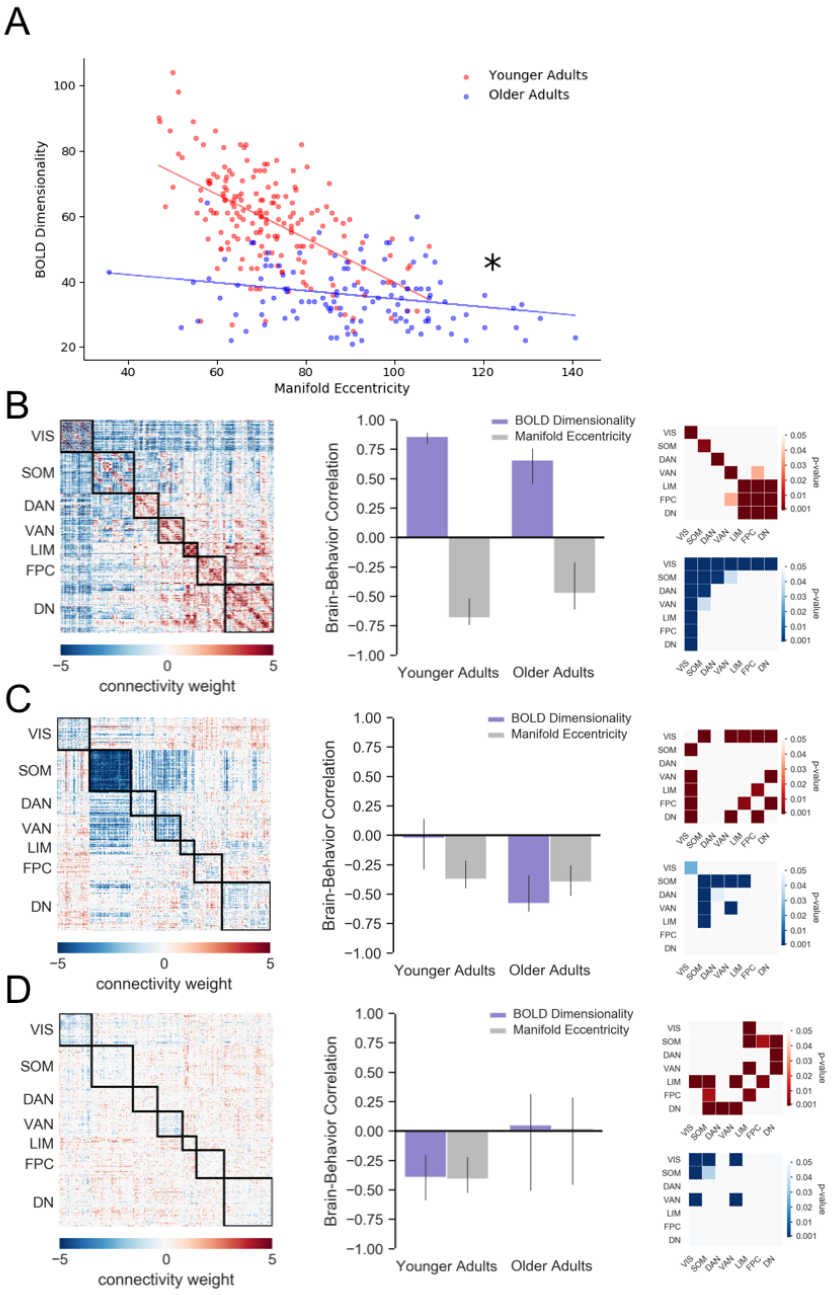

Figure 4 Caption: BOLD dimensionality and manifold eccentricity show converging and diverging patterns of RSFC. (A) Scatterplot showing the negative relationship between BOLD dimensionality and manifold eccentricity in younger ($r(179)$= -.575, p < .001, [-.64, -.50]) and older ($r(118)$= -.255, p < .005, [-.37, -.13]) adults. A star denotes a significantly stronger correlation in younger adults. (B-D) Three patterns of RSFC were related to BOLD dimensionality and manifold eccentricity. (B) Shared pattern of connectivity differentiating BOLD dimensionality and manifold eccentricity across age groups. (C) Overlap between BOLD dimensionality and manifold eccentricity in older adults as well as manifold eccentricity in younger adults. (D) Shared variance for BOLD dimensionality and manifold eccentricity in younger adults. VIS = visual, SOM= somatomotor, DAN= dorsal attention, VAN = ventral attention, LIM = limbic, FPC= frontoparietal, DN= default.

Aging & Cognition

Age-group differences in cognition were observed, consistent with cognitive aging (Park et al., 2002). Younger adults performed better on indices of episodic memory ($t(281)= 17.51$ $p < .001$; Cohen's $d = 2.11$), executive function ($t(281)= 12.67$, $p <.001$; Cohen's $d=1.52$), and processing speed ($t(281)= 15.03$, $p < .001$; Cohen's $d = 1.81$). Older adults had higher semantic memory index scores ($t(281)= 9.18$, $p < .001$; Cohen's $d = 1.10$; see Table 1 for descriptives).

BOLD Dimensionality, Manifold Eccentricity & Cognition

BOLD dimensionality demonstrated significant relationships with cognition (Table 2). In older adults, higher BOLD dimensionality was associated with higher episodic memory scores ($r(118)= .251$, $p < .01$, [.08, .41]). In younger adults, BOLD dimensionality showed a positive trending relationship with semantic memory ($r(161)= .155$, $p = .048$, [.00, .30]), which did not survive Bonferroni correction. Overlapping confidence intervals indicated no group differences in cognitive associations with BOLD dimensionality. Across the entire cohort, controlling for age, greater BOLD dimensionality was related to higher semantic memory scores (p$r(281) =.158$, $p < .01$, [.04, .27]) and lower executive function scores (p$r(281)= -.177$, $p <. 005$, [-.29, -.06]).

Manifold eccentricity associations with cognition were examined (Table 2). In younger adults, manifold eccentricity was negatively related to episodic memory ($r(161)= -.191$, $p < .05$, [-.34, -.04]) and processing speed ($r(161)= -.168$, $p < .05$, [-.31, -.01]), but neither correlation survived Bonferroni correction. No relationships were observed in older adults, and no relationships remained across the full sample when controlling for age.

Table 2: *BOLD Dimensionality and Manifold Eccentricity Correlations with Cognition*

Index	Younger Adults	Older Adults	Controlling for Age
BOLD Dimensionality			
Episodic Memory	.094 (.235)	**.251 (.006)***	.084 (.159)
Semantic Memory	.155 (.048)	.057 (.539)	**.158 (.008)***
Executive Function	-.146 (.062)	-.155 (.090)	**-.177 (.003)***
Processing Speed	.096 (.221)	-.018 (.848)	.016 (.784)
Manifold Eccentricity			
Episodic Memory	-.191 (.014)	-.073 (.430)	-.084 (.157)
Semantic Memory	-.134 (.088)	.020 (.832)	-.077(.196)
Executive Function	.040 (.609)	.094 (.305)	.085 (.154)
Processing Speed	-.168 (.032)	-.061 (.506)	-.080 (.182)

Note. r (*p*) values displayed.
* survives Bonferroni correction at p<.013.

Table 2 Note: Within younger and older adults, r (*p*) values displayed. When controlling for age, pr (*p*) values displayed. * survives Bonferroni correction at p<.013.

Brain Connectivity Scores & Cognition

Brain connectivity scores were extracted from the group-wise difference in connectivity (see **Connectomics** results above; Figure 3E) to interrogate how the observed pattern related to cognition. Higher brain connectivity scores for each age-group convey a stronger expression of the pattern of connectivity observed: greater within-network and lower between-network connectivity in younger adults; and lower within-network and greater between-network connectivity in older adults. Brain scores in younger adults were not reliably related to cognition, although a positive trending relationship with semantic memory was observed ($r(161)= .158$, $p = .044$, [.00, .03]; Table 3), which did not survive Bonferroni correction. Older adults' brain scores were negatively associated with executive function ($r(118)= -.350$, $p < .001$, [-.50, -.18]; Table 3). This indicates that greater between-network and lower within-network connectivity was negatively associated with executive function in older adults.

Dorsal Attention, Frontoparietal Control, and Default Sub-Network Connectomics

We further characterized age-group differences in functional connectivity among subnetworks of the default, frontoparietal control, and dorsal attention networks. Associations between sub-network RSFC age differences and behavior were also assessed.

Sub-Network Connectomics

The age-group average sub-network matrices are shown in Figure 5A-B. Older adults demonstrated fewer negative connections than younger adults, most visibly across DAN-A and DAN-B. The spring-embedded representation of the average top 5% of positive connections in each group (Figure 5C-D) suggests that older adults show more integration of the default network (DN-A) and frontoparietal control network (CONT-A).

Quantitative comparison of the inter-regional functional connectivity revealed a distinct pattern of age differences (permuted $p < 0.001$; 100% covariance explained; Figure 5E). Younger adults (Figure 5F) showed more within-network connectivity, and frontoparietal control to default connectivity (CONT-A to DN-A; CONT-A to DN-B; CONT-C to DN-C). Older adults (Figure 5G) showed greater between-network connectivity of the dorsal attention network (DAN-A) with all other sub-networks, as well as greater connectivity between the dorsal attention network (DAN-B) and the frontoparietal control (CONT-C) and default networks (DN-A). Older adults also showed greater connectivity between the frontoparietal control (CONT-C) and default network (DN-A). A similar pattern of connectivity was observed with a 200 parcellation scheme (Supplementary Figure 7).

Figure 5

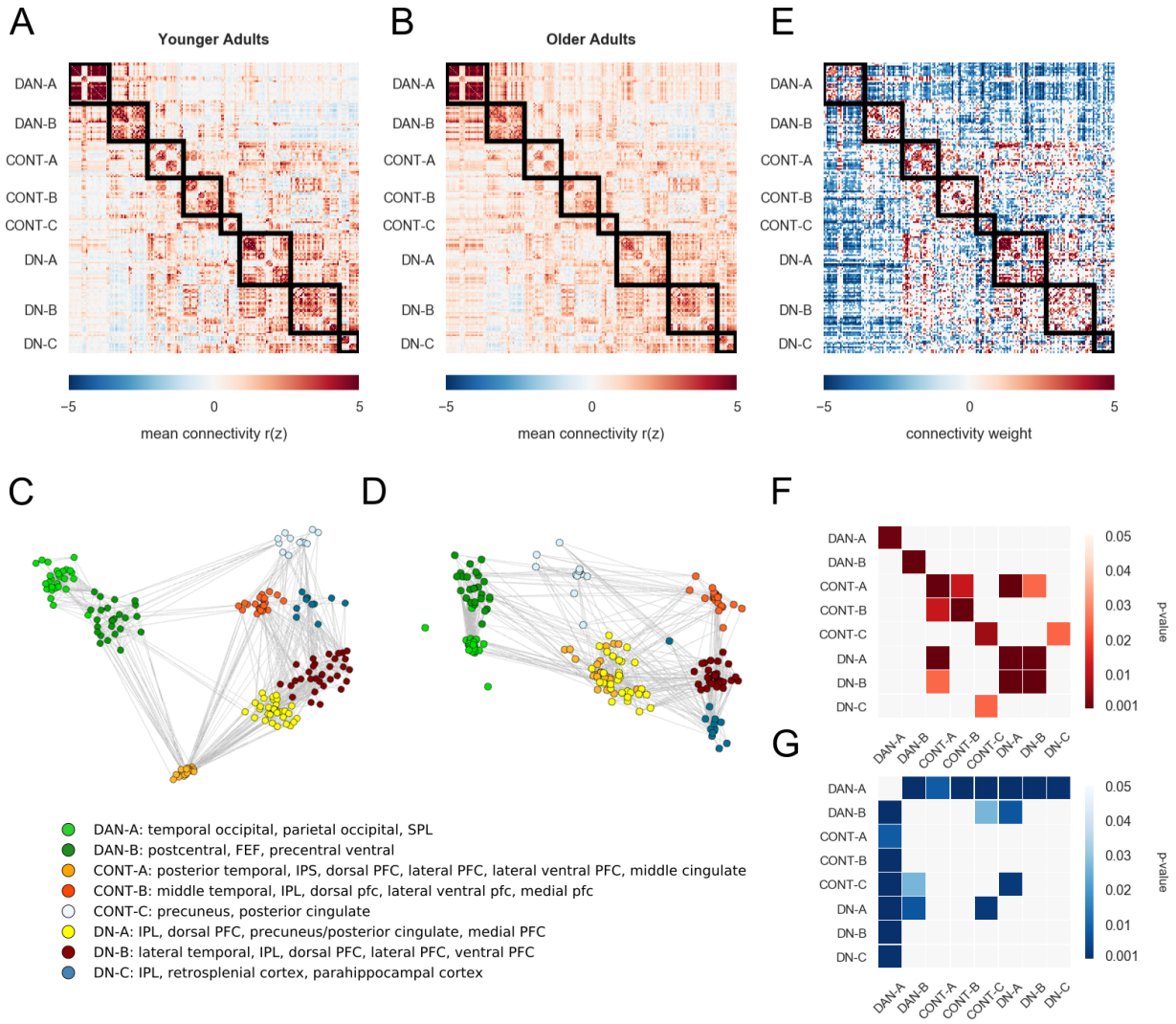

Figure 5 Caption: Functional connectivity of the dorsal attention (DAN), frontoparietal control (CONT), and default (DN) sub-networks following Yeo 17-network solution. Mean group connectivity in (A) younger and (B) older adults. Spring-embedded plots (5% edge density) of the mean correlation matrices for (C) younger and (D) older adults. (E) Differences in RSFC between younger and older adults among DAN, CONT, and DN. (F) Greater within- and between- network connectivity in young. (G) Greater within- and between- network connectivity in older adults.

Sub-Network Brain Connectivity Scores & Cognition

Brain connectivity scores were extracted from the group-wise difference in dorsal attention, frontoparietal control and default sub-network connectomics (Figure 5E) and related to cognition. Sub-network brain connectivity scores did not show any reliable associations with cognition in younger adults (Table 3). In older adults, sub-network brain connectivity scores demonstrated a negative association with executive function ($r(118)= .434$, $p < .001$, [-.57, -.28]; Table 3B).

Cross-Validation of the PLS Connectomics Findings

To verify that our results were not confounded by potential overfitting of the PLS model, the full and sub-network PLS analyses were run only on the first run of data. Brain connectivity scores were then computed from the run1-derived weights and the run2 individual-subject RSFC matrices and compared between groups. Age group differences were replicated in the held out run ($t(299)= 17.48$, $p < .001$, Cohen's $d= 2.06$). Additionally, brain connectivity scores derived from run2 were significantly correlated with executive function in older adults ($r(118)= -.366$, $p < .001$, [-.51,-.20]). In the sub-network analysis, age group differences were also replicated in the held out run ($t(299)= 19.46$, $p < .001$, Cohen's $d= 2.29$). Sub-network brain connectivity scores derived from run2 were also significantly correlated with executive function in older adults ($r(118)= -.425$, $p < .001$, [-.56,-.27]). These cross-validation analyses (see Supplementary Figure 8) demonstrate that the PLS results are robust to model overfitting.

Table 3: *Composite Brain Connectivity Score Associations with Cognition*

Index	Younger Adults	Older Adults
Whole Brain		
Episodic Memory	.039 (.624)	.139 (.131)
Semantic Memory	.158 (.044)	-.001 (.993)
Executive Function	-.145 (.064)	**-.350 (.000)***
Processing Speed	.128 (.103)	-.062 (.504)
Sub-network		
Episodic Memory	.007 (.928)	.070 (.445)
Semantic Memory	.138 (.079)	.048 (.601)
Executive Function	-.126 (.109)	**-.434 (.000)***
Processing Speed	.128 (.102)	-.116 (.206)

Note. r (*p*) values displayed.
Subnetworks encompass the dorsal attention, frontoparietal control and default networks.
* survives Bonferroni correction at p<.013.

Table 3 Note: r (*p*) values displayed. Subnetworks encompass the dorsal attention, frontoparietal control, and default networks. * survives Bonferroni correction at $p < .013$.

Discussion

Here we provide a comprehensive account of the intrinsic functional network architecture of the aging brain. Three methodological innovations—ME-fMRI acquisition with ME-ICA denoising, individual cortical parcellation, and multivariate statistical approaches (gradient mapping and Partial Least Squares)—were applied to address persistent and pervasive limitations in the field, offering a powerful lens into brain and cognitive aging. We identified several core features of brain aging. Dimensionality, the number of BOLD components in fMRI signal, was significantly lower for older versus younger adults. Macroscale connectivity gradients were largely age-invariant, revealing a principal gradient from primary to transmodal cortices and a secondary gradient from visual to somatomotor regions. Voxelwise coherence across these macroscale connectivity patterns, expressed in the gradient manifold, was reduced with age. Edge-level connectivity of canonical brain networks revealed a striking pattern of weaker within-network connectivity for older adults, in the context of stronger connectivity observed between visual and somatomotor regions and transmodal networks. An *a priori* analysis of transmodal networks revealed greater connectivity of the dorsal attention network to default and frontoparietal control networks for older adults, a pattern associated with lower executive control functioning. The collapse of within-network coherence and networkdedifferentiation are defining features of functional brain aging. In early development, network integration, leading to the formation of large-scale, spatially distributed brain networks is adaptive (Kundu et al., 2018) However, these findings suggest an inflection point (Zonneveld et al., 2019), with global network dedifferentiation becoming maladaptive in later life..

BOLD signal dimensionality

Dimensionality in the BOLD signal was significantly lower for older versus younger adults reflecting continued network dedifferentiation into later life. This finding extends an earlier report of cross-sectional dimensionality reductions from adolescence to early and middle adulthood (Kundu et al., 2018; Figure 1). Reductions in dimensionality in early adult development, largely attributable to functional integration among prefrontal and other transmodal cortices, reflects the transition from local connectivity to longer-range connections and the formation of spatially distributed yet intrinsically coherent brain networks (Kundu et al., 2018). The shift in functional brain organization parallels cognitive development over this period, which is marked by the emergence of more integrative and complex cognitive functions (Zelazo and Carlson, 2012), and is evident in the structural connectome organization during this period (Park et al., 2020). Our finding of an inverse relationship between dimensionality and executive functioning across the full sample, controlling for age, is consistent with this idea. Greater integration of distributed brain regions into intrinsically stable yet discrete functional networks, indexed here by lower dimensionality, provides the neural substrate necessary to support complex cognitive abilities across the lifespan (Bullmore et al., 2009). Controlling for age we also observed a positive association between BOLD signal dimensionality and semantic, or crystallized, knowledge. This correlation appears to be driven largely by the younger adult cohort (Table 2) and parallels the trajectory of cognitive development away from discrete, knowledge-dependent processing operations towards the emergence of more abstract, conceptual and schema-based integrative cognitive functions (Dumontheil, 2014; Ferrer et al., 2009). Within-group analyses revealed only a single positive correlation between dimensionality and

episodic memory in the older adult cohort. While speculative, this may reflect the integrity of the default network and its sub-network architecture in older adulthood (Andrews-Hanna et al., 2014). The medial temporal lobe subsystem, strongly implicated in episodic memory, is particularly vulnerable to age-related change (Buckner et al., 2005). The extent to which this subsystem is preserved as a distinct component of the default network, reflected as greater dimensionality in the BOLD signal, may support episodic memory performance into later life.

Few studies have investigated BOLD signal dimensionality as a marker of adult cognitive development, and we are not aware of any published work investigating these associations in older adulthood. As such, our interpretations of associations between dimensionality and cognitive abilities must be considered preliminary. What is clear from these findings is that the declines in the dimensionality of the BOLD signal, which begin in adolescence, continue unabated throughout adulthood and into later life. Lower dimensionality reflects greater functional integration and the emergence of large-scale brain networks in early development. However, the implications of progressive functional integration for brain and cognitive functioning into later life are less clear. Patterns of network dedifferntiation observed in our edge-level analysis were associated with lower executive control functioning, suggesting that continued network dedifferentiation may be maladaptive in older adulthood. Consistent with Kundu et al. (2018), BOLD signal dimensionality was derived as the number of BOLD components identified in the ME-fMRI time series. In single-echo fMRI and EEG investigations, estimations of signal dimensionality are instead obtained via Principal Component Analysis as the number of components needed to reproduce 80-90% of the neural signal. Using this latter approach, EEG signal dimensionality has been shown to increase as a function of age (e.g., McIntosh, Kovacevic & Itier, 2008). While preliminary, our findings point to the opposite direction, paving the path for future investigations into the use of multi-echo fMRI and different analytical approaches to derive signal dimensionality estimates.

Macroscale and edge-level functional connectivity

Next, we characterized both the macroscale functional architecture as well as edge-level differences in functional connectivity from younger to older adulthood. We provide the first demonstration that gradients are robust when using ME-ICA and recapitulate previous findings of connectivity gradients (Margulies et al., 2016). These reflect coherent shifts in functional connectivity from unimodal to transmodal association cortices (principal gradient) and from visual to somatomotor cortices (secondary gradient). Contrasting these gradient patterns for younger versus older adults revealed that the topography of both gradient patterns was largely preserved across age-cohorts. Despite the presence of age-related functional connectivity differences occurring within and between large-scale networks (see below), the macroscale architecture of cortical connectivity does not undergo substantial age-related change. We did observe higher gradient values in older adults than younger adults within the superior parietal lobule, indicating that this region is more closely affiliated with heteromodal cortex in older vs. younger adults. These findings are consistent with the edge-level connectivity analyses of reduced anticorrelation between the default and dorsal attention networks (see below; Spreng et al., 2016). We also observed significant differences in the cortex-wise dispersion of vertices in the principal-second gradient embedding space (i.e., manifold eccentricity). Older adults exhibit a less coherent voxelwise relationship between the two gradients across participants. While

greater manifold eccentricity for transmodal networks was weakly associated with poorer cognition in a previous report based on the CAM-CAN lifespan cohort (Bethlehem et al., 2020), we failed to find reliable associations with cognition in our sample.

We also adopted a partial least squares analytical approach to investigate age-differences across all edges in our 400 region parcellation. As PLS uses singular value decomposition to test age-differences across all edges in a single analytical step, we can report RSFC connectivity differences across the full 400x400 functional connectome, eliminating the need to apply functional connectivity strength or density thresholds. Visual inspection of the full connectomes for younger and older adults (Figure 3, Panels A-D) reveals a global pattern of network dedifferntiation for older versus younger adults, consistent with our dimensionality findings and previous reports (Betzel et al., 2014; Chan et al., 2014; Geerligs et al., 2015; Malagurski et al., 2020; Strumme et al., 2020). These qualitative differences were statistically validated in the PLS group analysis (Figure 3, Panel E) and aggregate network matrices (Figure 3, Panels F-G). Younger adults show a more robust pattern of within-network connectivity as well as between network connectivity of limbic, frontoparietal control, and default networks, consistent with the emergence of differentiated network organization in younger adulthood (Bullmore et al., 2009; Gratton et al., 2012).

Edge-level connectivity results revealed striking age differences. Older adults showed reduced within-network connectivity for all networks, as well as greater functional integration of the visual and somatomotor networks. Reduced within-network functional connectivity is a hallmark of normative aging (Damoiseaux, 2017 for a review). Interestingly, greater integration of visual and somatosensory regions with other networks is emerging as a feature of the aging connectome. Age-related increases in node participation, a graph analytic marker of functional integration, were limited to visual and somatosensory networks in a large study of age-differences in RSFC (Geerligs et al., 2015). More recently, Bethlehem and colleagues (2020) reported that practically all visual nodes moved closer to the center of all other networks in their gradient analysis. In a large sample of older adults, Stumme and colleagues (2020) observed that age-related differences in RSFC were most prominent in visual and somatosensory cortices, and these changes mediated cognitive abilities in their older adult sample. Intrinsic functional integration of visual regions within the broader connectome is consistent with task-based evidence suggesting greater top-down modulation of visual association cortices by transmodal regions in older adulthood. Greater activation of transmodal cortices, in the context of age-related declines in the fidelity of sensory signaling, has been interpreted as increased demands for top-down modulation of early sensory processing in later life (Clapp et al., 2011; Li and Rieckmann, 2014; Payer et al., 2006; Turner and D'Esposito, 2011). While beyond the scope of the current study, we speculate that task-driven increases in connectivity between transmodal and sensory cortices may shape the intrinsic functional architecture of these networks into later life.

Following from earlier work (Grady et al., 2016; Spreng et al., 2013; Sullivan et al., 2019), we also conducted a targeted analysis of age-differences in frontoparietal control, dorsal attention, and default networks. Younger adults showed greater within-network connectivity of all three networks. In contrast, older adults showed greater connectivity between the dorsal attention and the two other association networks. This pattern was particularly pronounced for a subnetwork of

the dorsal attention system (DAN-A) which includes the superior parietal lobule, the only region to show age differences in the gradient analysis. Reduced anti-correlations between these networks have previously been reported in older adults (Keller et al., 2015; Spreng et al., 2016). Interestingly, the DAN-A sub-network encompasses regions of the frontal, parietal and temporal cortices implicated in top-down, or goal-directed, attentional control. This is again consistent with a neuromodulatory account of neurocognitive aging, wherein greater allocation of attentional resources may be engaged to sharpen perceptual representations in later life (Li et al., 2006; Li and Rieckmann, 2014).

A neuromodulation account is well aligned with our finding that the expression of these age-related connectivity patterns was associated with poorer executive functioning for older adults. Reduced network segregation has previously been implicated in age-related cognitive decline (Betzel et al., 2014; Chan et al., 2014, Malagurski et al., 2020; Stumme et al., 2020). Our edge-level connectivity analyses suggest that greater integration of visual and dorsal attention regions with transmodal networks is insufficient to sustain complex cognition in later life. Notably, a differentiated functional architecture, while robustly manifest in our younger cohort, was not associated with younger adult performance for any of the cognitive domains assessed here. This suggests that the behavioral relevance of the intrinsic network architecture of the brain, shaped by repeated co-activation of neural circuits over a lifetime of learning and lived experience (Stevens and Spreng, 2014), may increase with advancing age. We have argued that these behavioral associations become more robust as intrinsic networks are continuously shaped by lifelong learning, knowledge accumulation, and experiences accrued over the adult lifespan (Spreng and Turner, 2019).

Finally, by combining multi-echo fMRI and PLS we were able to provide a more definitive view of age-differences in whole-brain connectomics. With ME-ICA, negative correlations are not a spurious byproduct of preprocessing but may reveal biologically meaningful information (Kundu et al., 2017). PLS determines edge-level differences in a single analytic step, eliminating the need for multiple comparisons correction (Krishnan et al., 2011). Common approaches to studying the intrinsic functional connectome, including independent components analysis and graph analytic techniques, often rely on post-hoc component labeling and arbitrary thresholding methods. These idiosyncratic decisions can mask subtle yet meaningful findings, influencing data interpretation and conclusions with respect to global differences in the functional connectome. A clear example of the potential distortions imposed by thresholding can be seen in Figure 3 (panels C, D). The figures display the young and old functional connectomes as spring-embedded graphs, reflecting the top 5% of positive connection strengths. Visual inspection of these graphs suggests relatively little change in the RSFC profile of visual and somatosensory networks from young to older adulthood. However, when accounting for the full connectome, including all positive and negative connection weights (Figure 3, panels E-G), it is clear that altered connectivity profiles of visual and somatomotor networks are a prominent feature of functional brain aging. A similar pattern can be seen for the transmodal network analyses (Figure 5). Reduced anti-correlation between dorsal attention and default brain regions, commonly observed in later life (Spreng and Stevens, 2016), and reflected in the full connectome (panels E-G), are not reflected in the spring-embedded graphs.

Previous investigations have informed our understanding of the functional architecture of the aging brain. However, thresholding may also serve to highlight specific connectivity patterns that can be obscured when analyzing the full edge-level connectome. Looking again at the thresholded, spring-embedded graphs in Figure 5 (panels C-D), one of the most striking age differences is greater coupling of default and frontoparietal control regions (DN-A to Control-A). We have previously characterized this as the Default to Executive Coupling Hypothesis of Aging (DECHA, Turner and Spreng, 2015; Spreng and Turner, 2019), and suggest that this between network pattern is associated with the shifting architecture of cognition in later life (Spreng et al., 2018) with both adaptive and maladaptive consequences for cognitive aging. Notably, this DECHA pattern is obscured in the full matrix analyses (Figure 5, panels F-G). Further, core features of functional networks in older adulthood have been discovered using these thresholded-based approaches (Chan et al., 2014; Geerligs et al., 2015), many of which we recapitulate here. Taken together, these findings suggest that the full and thresholded matrices reveal different features of the aging connectome and promote the adoption of both approaches in future investigations.

BOLD dimensionality, functional connectivity and behavior

We observed robust patterns of network dedifferentiation for older versus younger adults. This is consistent with our observation of lower BOLD signal dimensionality with advancing age. Interestingly, lower BOLD dimensionality was associated with better executive functioning in the whole sample, whereas network dedifferentiation (also associated with lower dimensionality) was associated with poorer executive functioning for older adults. This difference in behavioral associations hints at a more complex relationship between BOLD dimensionality and network dedifferentiation in older adulthood. While speculative, we suggest that late-life reductions in BOLD signal dimensionality may reflect the temporal unfolding of two divergent connectivity patterns. The first is a 'young-like' pattern, positively associated with BOLD dimensionality. This pattern reflects the relative preservation of a modular network architecture into older age (Figure 4, panel B), optimized to support complex cognition. With advancing age, this modular network architecture collapses. Here, lower BOLD dimensionality reflects the loss of within network connections and global network dedifferentiation (Figure 4, Panel C). Greater expression of the latter pattern represents maladaptive network reorganization, associated with lower executive functioning in later life. This interpretation is consistent with the recent suggestion that functional integration may reach an inflection point in middle adulthood, marking a shift from cognitive resilience to cognitive decline (Zonneveld et al., 2019). Tracing these trajectories of BOLD dimensionality and associations with network connectivity and complex cognition across the lifespan will be an important direction for future work.

Conclusion

We designed and deployed a multi-echo fMRI protocol in combination with individualized parcellation methods and novel analytical approaches to comprehensively characterize the functional architecture of the aging brain. We report significant reductions in BOLD signal dimensionality extending into later life. Large-scale functional connectivity gradients are mostly preserved with age. However, striking age differences were observed in edge-level connectivity patterns. Aging RSFC was marked by lower within- and greater between- network connectivity,

including the striking integration of visual and somatomotor regions with higher-order association networks. These findings implicate network dedifferentiation, reflected here as reduced dimensionality within the BOLD signal and altered edge-level connectivity, as a global and putatively maladaptive feature of functional brain aging. However, greater coherence among specific networks (e.g. default - frontoparietal control; Spreng & Turner, 2019) may also signal adaptive functional reorganization in later life. By overcoming persistent and pervasive methodological challenges that have confounded previous research, the results provide a comprehensive account of the intrinsic functional architecture of the aging brain.

The methodological and analytical innovations implemented here ameliorated several of the most pervasive and enduring challenges in lifespan network neuroscience. These include age-related variability in noise profiles within the BOLD signal, as well as distortions introduced by group-wise spatial alignment to standardized templates. Of course, ME-fMRI protocols and individualized parcellations cannot address the totality of confounds that complicate cross-sectional data analyses. Among the most critical issues remaining involves resolving, or at least accurately modeling, age differences in neurovascular coupling. Altered neurovascular coupling with age can introduce spurious RSFC differences that are difficult to detect with standard imaging protocols (Tsvetanov et al., 2020 for a review). While ME-ICA methods, which separate neural from non-neural sources in the BOLD signal, are a significant advance, implementation of multimodal methods such as simultaneous arterial spin labeling and echo-planar imaging may be necessary to resolve this issue (Tsvetanov et al., 2020). Despite these limitations, we suggest that the methodological innovations implemented here provide a comprehensive, multi-faceted, and high-fidelity representation of age-differences in the functional network architecture of the brain. Taken together, the findings add much needed clarity and precision to the current understanding of how functional networks are formed, shaped, and degraded in older adulthood.

Acknowledgments
This work was supported in part by NIH Grant 1S10RR025145 and by a Canadian Institute of Health Research grant to R.N.S..

Declaration of Interests
The authors declare no competing interests.

References

Alexander-Bloch, A. F., Shou, H., Liu, S., Satterthwaite, T. D., Glahn, D. C., Shinohara, R. T., . Raznahan, A. (2018). On testing for spatial correspondence between maps of human brain structure and function. Neuroimage, 178, 540-551.

Andrews-Hanna, J. R., Smallwood, J., & Spreng, R. N. (2014). The default network and self-generated thought: Component processes, dynamic control, and clinical relevance. *Annals of the New York Academy of Sciences*, *1316*(1), 29–52. https://doi.org/10.1111/nyas.12360

Andrews-Hanna, J. R., Snyder, A. Z., Vincent, J. L., Lustig, C., Head, D., Raichle, M. E., & Buckner, R. L. (2007). Disruption of large-scale brain systems in advanced aging. *Neuron*, *56*(5), 924–935. https://doi.org/10.1016/j.neuron.2007.10.038

Austin, P. C., & Hux, J. E. (2002). A brief note on overlapping confidence intervals. *Journal of Vascular Surgery*, *36*(1), 194–195. https://doi.org/10.1067/mva.2002.125015

Beck, A.T., Steer, R.A., & Brown, G.K. (1996). Manual for the Beck Depression Inventory-II. San Antonio, TX: Psychological Corporation

Bethlehem, R. A. I., Paquola, C., Seidlitz, J., Ronan, L., Bernhardt, B., Consortium, C. C. A. N., & Tsvetanov, K. A. (2020). Dispersion of functional gradients across the adult lifespan. *NeuroImage*, *222*(July), 117299. https://doi.org/10.1016/j.neuroimage.2020.117299

Betzel, R. F., Byrge, L., He, Y., Goñi, J., Zuo, X. N., & Sporns, O. (2014). Changes in structural and functional connectivity among resting-state networks across the human lifespan. *NeuroImage*, *102 Pt 2*, 345–357. https://doi.org/10.1016/j.neuroimage.2014.07.067

Braga, R. M., & Buckner, R. L. (2017). Parallel Interdigitated Distributed Networks within the Individual Estimated by Intrinsic Functional Connectivity. *Neuron*, *95*(2), 457–471.e5. https://doi.org/10.1016/j.neuron.2017.06.038

Brainerd, C. J., Reyna, V. F., Gomes, C. F., Kenney, A. E., Gross, C. J., Taub, E. S., Spreng, R. N., & Alzheimer's Disease Neuroimaging Initiative (2014). Dual-retrieval models and neurocognitive impairment. *Journal of experimental psychology. Learning, memory, and cognition*, *40*(1), 41–65. https://doi.org/10.1037/a0034057

Buckner, R. L., Head, D., Parker, J., Fotenos, A. F., Marcus, D., Morris, J. C., & Snyder, A. Z. (2004). A unified approach for morphometric and functional data analysis in young, old, and demented adults using automated atlas-based head size normalization: Reliability and validation against manual measurement of total intracranial volume. *NeuroImage*, *23*(2), 724–738. https://doi.org/10.1016/j.neuroimage.2004.06.018

Buckner, R. L., Snyder, A. Z., Shannon, B. J., LaRossa, G., Sachs, R., Fotenos, A. F., … Mintun, M. A. (2005). Molecular, structural, and functional characterization of Alzheimer's disease:

Evidence for a relationship between default activity, amyloid, and memory. *Journal of Neuroscience*, *25*(34), 7709–7717. https://doi.org/10.1523/JNEUROSCI.2177-05.2005

Chan, M. Y., Park, D. C., Savalia, N. K., Petersen, S. E., & Wig, G. S. (2014). Decreased segregation of brain systems across the healthy adult lifespan. *Proceedings of the National Academy of Sciences of the United States of America*, *111*(46), E4997–E5006. https://doi.org/10.1073/pnas.1415122111

Chong, M., Bhushan, C., Joshi, A. A., Choi, S., Haldar, J. P., Shattuck, D. W., … Leahy, R. M. (2017). Individual parcellation of resting fMRI with a group functional connectivity prior. NeuroImage, 156(May), 87–100. https://doi.org/10.1016/j.neuroimage.2017.04.054

Clapp, W. C., Rubens, M. T., Sabharwal, J., & Gazzaley, A. (2011). Deficit in switching between functional brain networks underlies the impact of multitasking on working memory in older adults. *Proceedings of the National Academy of Sciences of the United States of America*, *108*(17), 7212–7217. https://doi.org/10.1073/pnas.1015297108

Coifman, R. R., Lafon, S., Lee, A. B., Maggioni, M., Nadler, B., Warner, F., & Zucker, S. W. (2005). Geometric diffusions as a tool for harmonic analysis and structure definition of data: Diffusion maps. Proceedings of the National Academy of Sciences of the United States of America, 102(21), 7426–7431. https://doi.org/10.1073/pnas.0500334102

Damoiseaux J. S. (2017). Effects of aging on functional and structural brain connectivity. *NeuroImage*, *160*, 32–40. https://doi.org/10.1016/j.neuroimage.2017.01.077

Daneman, M., & Carpenter, P. A. (1980). Individual differences in working memory and reading. *Journal of Verbal Learning and Verbal Behavior, 19*(4), 450. Retrieved from https://proxy.library.mcgill.ca/login?url=https://search.proquest.com/docview/1297349869?accountid=12339

Doucet, G. E., Labache, L., Thompson, P. M., Joliot, M., & Frangou, S. (2020). Atlas55+: Brain Functional Atlas of Resting-State Networks for Late Adulthood. *Cerebral Cortex*, 1–13. https://doi.org/10.1093/cercor/bhaa321

Dumontheil I. (2014). Development of abstract thinking during childhood and adolescence: the role of rostrolateral prefrontal cortex. *Developmental cognitive neuroscience*, *10*, 57–76. https://doi.org/10.1016/j.dcn.2014.07.009

Eickhoff, S. B., Yeo, B. T. T., & Genon, S. (2018). Imaging-based parcellations of the human brain. *Nature Reviews Neuroscience*, *19*(11), 672–686. https://doi.org/10.1038/s41583-018-0071-7

Efron, B., & Tibshirani, R. (1986). Bootstrap methods for standard errors, confidence intervals, and other measures of statistical accuracy. *Statistical Science*, *1*(1), 54–75. https://doi.org/10.1214/ss/1177013815

Felleman, D. J., & Van Essen, D. C. (1991). Distributed hierarchical processing in the primate cerebral cortex. *Cerebral cortex (New York, N.Y. : 1991)*, *1*(1), 1–47. https://doi.org/10.1093/cercor/1.1.1

Ferrer, E., O'Hare, E. D., & Bunge, S. A. (2009). Fluid reasoning and the developing brain. *Frontiers in Neuroscience*, *3*(MAY), 46–51. https://doi.org/10.3389/neuro.01.003.2009

Fox, M. D., & Raichle, M. E. (2007). Spontaneous fluctuations in brain activity observed with functional magnetic resonance imaging. *Nature Reviews. Neuroscience*, *8*(9), 700–711. https://doi.org/10.1038/nrn2201

Fischl, B. (2012). FreeSurfer. NeuroImage, 62(2), 774–781. https://doi.org/10.1016/j.neuroimage.2012.01.021

Folstein, M. F., Folstein, S. E., & McHugh, P. R. (1975). "Mini-Mental State" A practical method for grading the cognitive state of patients for the clinician. Journal of Psychiatric Research, 12, 189–198. http://doi.org/10.1016/0022-3956(75)90026-6

Ge, T., Holmes, A.J., Buckner, R.L., Smoller, J.W., Sabuncu, M.R. (2017). Heritability analysis with repeat measurements and its application to resting-state functional connectivity. Proceedings of the National Academy of Sciences, 114(21), 5521–6. https://doi.org/10.1073/pnas.1700765114.

Geerligs, L., Renken, R. J., Saliasi, E., Maurits, N. M., & Lorist, M. M. (2015). A brain-wide study of age-related changes in functional connectivity. *Cerebral Cortex*, *25*(7), 1987–1999. https://doi.org/10.1093/cercor/bhu012

Gershon, R. C., Wagster, M. V., Hendrie, H. C., Fox, N. A., Cook, K. F., & Nowinski, C. J. (2013). NIH toolbox for assessment of neurological and behavioral

Girn, M., Roseman, L., Bernhardt, B., Smallwood, J., Carhart-Harris, R. L., & Spreng, N. R. (2020). LSD flattens the functional hierarchy of the human brain. Bioarxiv. doi:10.1101/2020.05.01.072314

Glover, G.H., Li, T.-Q. and Ress, D. (2000), Image-based method for retrospective correction of physiological motion effects in fMRI: RETROICOR. Magn. Reson. Med., 44: 162-167. https://doi.org/10.1002/1522-2594(200007)44:1.

Gotts, S. J., Gilmore, A. W., & Martin, A. (2020). Brain networks, dimensionality, and global signal averaging in resting-state fMRI: Hierarchical network structure results in low-dimensional spatiotemporal dynamics. *NeuroImage*, *205*, 116289. https://doi.org/10.1016/j.neuroimage.2019.116289

Gordon, E. M., Laumann, T. O., Adeyemo, B., Gilmore, A. W., Nelson, S. M., Dosenbach, N., & Petersen, S. E. (2017). Individual-specific features of brain systems identified with

resting state functional correlations. *NeuroImage*, *146*, 918–939. https://doi.org/10.1016/j.neuroimage.2016.08.032

Grady, C., Sarraf, S., Saverino, C., & Campbell, K. (2016). Age differences in the functional interactions among the default, frontoparietal control, and dorsal attention networks. *Neurobiology of Aging*, *41*, 159–172. https://doi.org/10.1016/j.neurobiolaging.2016.02.020

Gratton, C., Nomura, E. M., Pérez, F., & D'Esposito, M. (2012). Focal brain lesions to critical locations cause widespread disruption of the modular organization of the brain. *Journal of cognitive neuroscience*, *24*(6), 1275–1285. https://doi.org/10.1162/jocn_a_00222

Greicius, M. D., Srivastava, G., Reiss, A. L., & Menon, V. (2004). Default-mode network activity distinguishes Alzheimer's disease from healthy aging: evidence from functional MRI. *Proceedings of the National Academy of Sciences of the United States of America*, *101*(13), 4637–4642. https://doi.org/10.1073/pnas.0308627101

Greve, D. N., & Fischl, B. (2009). Accurate and robust brain image alignment using boundary-based registration. NeuroImage, 48(1), 63–72. https://doi.org/10.1016/j.neuroimage.2009.06.060

Haxby, J. V., Guntupalli, J. S., Connolly, A. C., Halchenko, Y. O., Conroy, B. R., Gobbini, M. I., … Ramadge, P. J. (2011). A common, high-dimensional model of the representational space in human ventral temporal cortex. *Neuron*, *72*(2), 404–416. https://doi.org/10.1016/j.neuron.2011.08.026

Hong, S.-J., de Wael, R. V., Bethlehem, R. A., Lariviere, S., Paquola, C., Valk, S. L., . . . Smallwood, J. (2019). Atypical functional connectome hierarchy in autism. Nature communications, 10(1), 1022.

Jo, H. J., Saad, Z. S., Simmons, W. K., Milbury, L. A., & Cox, R. W. (2010). Mapping sources of correlation in resting state FMRI, with artifact detection and removal. *NeuroImage*, *52*(2), 571–582. https://doi.org/10.1016/j.neuroimage.2010.04.246

Kaas J. H. (1987). The organization of neocortex in mammals: implications for theories of brain function. *Annual review of psychology*, *38*, 129–151. https://doi.org/10.1146/annurev.ps.38.020187.001021

Keller, J. B., Hedden, T., Thompson, T. W., Anteraper, S. A., Gabrieli, J. D., & Whitfield-Gabrieli, S. (2015). Resting-state anticorrelations between medial and lateral prefrontal cortex: association with working memory, aging, and individual differences. *Cortex; a journal devoted to the study of the nervous system and behavior*, *64*, 271–280. https://doi.org/10.1016/j.cortex.2014.12.001

Kong, R., Li, J., Orban, C., Sabuncu, M. R., Liu, H., Schaefer, A., … Yeo, B. T. T. (2019). Spatial Topography of Individual-Specific Cortical Networks Predicts Human Cognition, Personality, and Emotion. Cerebral Cortex, 29(6), 2533–2551. https://doi.org/10.1093/cercor/bhy123

Krishnan, A., Williams, L. J., McIntosh, A. R., & Abdi, H. (2011). Partial Least Squares (PLS) methods for neuroimaging: a tutorial and review. *NeuroImage*, *56*(2), 455–475. https://doi.org/10.1016/j.neuroimage.2010.07.034

Kundu, P., Santin, M. D., Bandettini, P. a., Bullmore, E. T., & Petiet, A. (2011). Differentiating BOLD and non-BOLD signals in fMRI time series using multi-echo EPI. NeuroImage, 60, 1759–1770.

Kundu, P., Brenowitz, N. D., Voon, V., Worbe, Y., Vértes, P. E., Inati, S. J., … Bullmore, E. T. (2013). Integrated strategy for improving functional connectivity mapping using multiecho fMRI. Proceedings of the National Academy of Sciences of the Unites States of America, 110(40), 16187–16192. http://doi.org/10.1073/pnas.1301725110

Kundu, P., Voon, V., Balchandani, P., Lombardo, M. V., Poser, B. A., & Bandettini, P. A. (2017). Multi-echo fMRI: A review of applications in fMRI denoising and analysis of BOLD signals. NeuroImage, 154(March), 59–80. https://doi.org/10.1016/j.neuroimage.2017.03.033

Kundu, P., Benson, B. E., Rosen, D., Frangou, S., Leibenluft, E., Luh, W. M., … Ernst, M. (2018). The integration of functional brain activity from adolescence to adulthood. Journal of Neuroscience, 38(14), 3559–3570. https://doi.org/10.1523/JNEUROSCI.1864-17.2018

Laumann, T. O., Gordon, E. M., Adeyemo, B., Snyder, A. Z., Joo, S. J., Chen, M. Y., Gilmore, A. W., McDermott, K. B., Nelson, S. M., Dosenbach, N. U., Schlaggar, B. L., Mumford, J. A., Poldrack, R. A., & Petersen, S. E. (2015). Functional System and Areal Organization of a Highly Sampled Individual Human Brain. *Neuron*, *87*(3), 657–670. https://doi.org/10.1016/j.neuron.2015.06.037

Li, J., Kong, R., Liégeois, R., Orban, C., Tan, Y., Sun, N., Holmes, A. J., Sabuncu, M. R., Ge, T., & Yeo, B. (2019). Global signal regression strengthens association between resting-state functional connectivity and behavior. *NeuroImage*, *196*, 126–141. https://doi.org/10.1016/j.neuroimage.2019.04.016

Li, S. C., & Rieckmann, A. (2014). Neuromodulation and aging: implications of aging neuronal gain control on cognition. *Current opinion in neurobiology*, *29*, 148–158. https://doi.org/10.1016/j.conb.2014.07.009

Madden, D. J., Jain, S., Monge, Z. A., Cook, A. D., Lee, A., Huang, H., Howard, C. M., & Cohen, J. R. (2020). Influence of structural and functional brain connectivity on age-related differences in fluid cognition. *Neurobiology of aging*, *96*, 205–222. https://doi.org/10.1016/j.neurobiolaging.2020.09.010

Malagurski, B., Liem, F., Oschwald, J., Mérillat, S., & Jäncke, L. (2020). Functional dedifferentiation of associative resting state networks in older adults – A longitudinal study. *NeuroImage*, *214*(February). https://doi.org/10.1016/j.neuroimage.2020.116680

Margulies, D. S., Ghosh, S. S., Goulas, A., Falkiewicz, M., Huntenburg, J. M., Langs, G., . . . Petrides, M. (2016). Situating the default-mode network along a principal gradient of macroscale cortical organization. Proceedings of the National Academy of Sciences, 113(44), 12574-12579.

McIntosh, A. R., & Lobaugh, N. J. (2004). Partial least squares analysis of neuroimaging data: Applications and advances. NeuroImage, 23, 250–263. https://doi.org/10.1016/j.neuroimage.2004.07.020

McIntosh, A.R., Mišić, B. (2013). Multivariate statistical analyses for neuroimaging data. Annual Review of Psychology, 64(1), 499–525. https://doi.org/10.1146/annurev- psych-113011- 143804.

Mwilambwe-Tshilobo, L., Ge, T., Chong, M., Ferguson, M. A., Misic, B., Burrow, A. L., … Spreng, R. N. (2019). Loneliness and meaning in life are reflected in the intrinsic network architecture of the brain. Social Cognitive and Affective Neuroscience, 14(4), 423–433. https://doi.org/10.1093/scan/nsz021

Mrvar, A., & Batagelj, V. (2016). Analysis and visualization of large networks with program package Pajek. *Complex Adaptive Systems Modeling*, *4*(1). https://doi.org/10.1186/s40294-016-0017-8

Park, B.-y., Bethlehem, R. A., Paquola, C., Lariviere, S., Cruces, R. R., de Wael, R. V., . . . Bernhardt, B. (2020). Macroscale connectome manifold expansion in adolescence. bioRxiv. https://www.biorxiv.org/content/10.1101/2020.06.22.165621v2

Parkes, L., Fulcher, B., Yücel, M., & Fornito, A. (2018). An evaluation of the efficacy, reliability, and sensitivity of motion correction strategies for resting-state functional MRI. NeuroImage, 171(July 2017), 415–436. https://doi.org/10.1016/j.neuroimage.2017.12.073

Payer, D., Marshuetz, C., Sutton, B., Hebrank, A., Welsh, R. C., & Park, D. C. (2006). Decreased neural specialization in old adults on a working memory task. *Neuroreport*, *17*(5), 487–491. https://doi.org/10.1097/01.wnr.0000209005.40481.31

Power, J. D., Barnes, K. A., Snyder, A. Z., Schlaggar, B. L., & Petersen, S. E. (2012). Spurious but systematic correlations in functional connectivity MRI networks arise from subject motion. NeuroImage, 59(3), 2142–2154. https://doi.org/10.1016/j.neuroimage.2011.10.018

Power, J. D., Plitt, M., Gotts, S. J., Kundu, P., Voon, V., Bandettini, P. A., & Martin, A. (2018). Ridding fMRI data of motion-related influences: Removal of signals with distinct spatial and physical bases in multiecho data. *Proceedings of the National Academy of Sciences of the United States of America*, *115*(9), E2105–E2114. https://doi.org/10.1073/pnas.1720985115

Reitan, R. M. (1958). Validity of the Trail Making Test as an indicator of organic brain damage. *Perceptual and Motor Skills, 8,* 271–276. https://doi.org/10.2466/PMS.8.7.271-276

Saad, Z. S., Gotts, S. J., Murphy, K., Chen, G., Jo, H. J., Martin, A., & Cox, R. W. (2012). Trouble at rest: how correlation patterns and group differences become distorted after global signal regression. *Brain connectivity*, *2*(1), 25–32. https://doi.org/10.1089/brain.2012.0080

Saad, Z. S., Reynolds, R. C., Jo, H. J., Gotts, S. J., Chen, G., Martin, A., & Cox, R. W. (2013). Correcting brain-wide correlation differences in resting-state FMRI. *Brain connectivity*, *3*(4), 339–352. https://doi.org/10.1089/brain.2013.0156

Samanez-Larkin, G. R., & D'Esposito, M. (2008). Group comparisons: Imaging the aging brain. Social Cognitive and Affective Neuroscience, 3(3), 290–297. https://doi.org/10.1093/scan/nsn029

Schaefer, A., Kong, R., Gordon, E. M., Laumann, T. O., Zuo, X.-N., Holmes, A. J., … Yeo, B. T. T. (2018). Local-global parcellation of the human cerebral cortex from intrinsic functional connectivity MRI. Cerebral Cortex, 28, 3095–3114. https://doi.org/10.1093/cercor/bhx179

Shafiei, G., Zeighami, Y., Clark, C. A., Coull, J. T., Nagano-Saito, A., Leyton, M., ... & Mišić, B. (2019). Dopamine signaling modulates the stability and integration of intrinsic brain networks. *Cerebral Cortex*, *29*(1), 397-409.

Shipley, W. C., Gruber, C. P, Martin, T. A., & Klein, A. M. (2009). *Shipley-2 manual*. Los Angeles, CA: Western Psychological Services.

Smith, A. (1982). *Symbol Digit Modalities Test (SDMT) manual (revised)*.

Smith, S. M. (2002). Fast robust automated brain extraction. Human Brain Mapping, 17(3), 143–155. http://doi.org/10.1002/hbm.10062

Speck, O., Ernst, T., Chang, L., 2001. Biexponential modeling of multigradient-echo MRI data of the brain. Magn. Reson. Med. 45, 1116–1121. http://dx.doi.org/10.1002/ mrm.1147.

Spreng, R. N., Fernández-Cabello, S., Turner, G. R., & Stevens, W. D. (2019). Take a deep breath: Multiecho fMRI denoising effectively removes head motion artifacts, obviating the need for global signal regression. *Proceedings of the National Academy of Sciences of the United States of America*, *116*(39), 19241–19242. https://doi.org/10.1073/pnas.1909848116

Spreng, R. N., Stevens, W. D., Viviano, J. D., & Schacter, D. L. (2016). Attenuated anticorrelation between the default and dorsal attention networks with aging: evidence from task and rest. *Neurobiology of aging*, *45*, 149–160. https://doi.org/10.1016/j.neurobiolaging.2016.05.020

Spreng, R. N., & Turner, G. R. (2013). Structural covariance of the default network in healthy and pathological aging. *The Journal of Neuroscience : The Official Journal of the Society for Neuroscience*, *33*(38), 15226–15234. https://doi.org/10.1523/JNEUROSCI.2261-13.2013

Spreng, R. N., & Turner, G. R. (2019). The shifting architecture of cognition and brain function in older adulthood. *Perspectives on Psychological Science*. Retrieved from http://citeseerx.ist.psu.edu/viewdoc/download?doi=10.1.1.169.5067&rep=rep1&type=pdf

Stevens, W. D., & Spreng, R. N. (2014). Resting-state functional connectivity MRI reveals active processes central to cognition. *Wiley Interdisciplinary Reviews: Cognitive Science*, *5*(2), 233–245. https://doi.org/10.1002/wcs.1275

Stumme, J., Jockwitz, C., Hoffstaedter, F., Amunts, K., & Caspers, S. (2020). Functional network reorganization in older adults: Graph-theoretical analyses of age, cognition and sex. *NeuroImage*, *214*(February). https://doi.org/10.1016/j.neuroimage.2020.116756

Sullivan, M. D., Anderson, J., Turner, G. R., Spreng, R. N., & Alzheimer's Disease Neuroimaging Initiative (2019). Intrinsic neurocognitive network connectivity differences between normal aging and mild cognitive impairment are associated with cognitive status and age. *Neurobiology of aging*, *73*, 219–228. https://doi.org/10.1016/j.neurobiolaging.2018.10.001

Tsvetanov, K. A., Henson, R. N. A., Jones, P. S., Mutsaerts, H., Fuhrmann, D., Tyler, L. K., & Rowe, J. B. (2020). The effects of age on resting-state BOLD signal variability is explained by cardiovascular and cerebrovascular factors. *Psychophysiology*, (September 2019), 1–20. https://doi.org/10.1111/psyp.13714

Turner, G., & D'Esposito, M. (2014). Neurorehabilitation of executive functions. In M. Selzer, S. Clarke, L. Cohen, G. Kwakkel, & R. Miller (Eds.), *Textbook of Neural Repair and Rehabilitation* (pp. 489-499). Cambridge: Cambridge University Press. doi:10.1017/CBO9780511995590.042

Vos de Wael, R., Benkarim, O., Paquola, C. et al. BrainSpace: a toolbox for the analysis of macroscale gradients in neuroimaging and connectomics datasets. Commun Biol 3, 103 (2020). https://doi.org/10.1038/s42003-020-0794-7

Wang, D., Buckner, R. L., Fox, M. D., Holt, D. J., Holmes, A. J., Stoecklein, S., Langs, G., Pan, R., Qian, T., Li, K., Baker, J. T., Stufflebeam, S. M., Wang, K., Wang, X., Hong, B., & Liu,

H. (2015). Parcellating cortical functional networks in individuals. *Nature neuroscience*, *18*(12), 1853–1860. https://doi.org/10.1038/nn.4164

Wechsler, D. (2009). *Wechsler Memory Scale (Fourth Edition).* San Antonio, TX: Pearson.

Worsley, K.J., Taylor JE, Carbonell F, Chung MK, Duerden E, Bernhardt B, Lyttelton O, Boucher M, Evans (2009). SurfStat: A Matlab toolbox for the statistical analysis of univariate and multivariate surface and volumetric data using linear mixed effects models and random field theory. *NeuroImage*, 47, Supplement 1, S102, https://doi.org/10.1016/S1053-8119(09)70882-1.

Yeo, B. T. T., Kirienen, F. M., Sepulcre, J., Sabuncu, M. R., Lashkari, D., Hollinshead, M., . . . Buckner, R. L. (2011). The organization of the human cerebral cortex estimated by intrinsic functional connectivity. J Neurophysiol, 106, 1125-1165. doi:10.1152/jn.00338.2011.

Yesavage, J. A., & Brink, T. L. (1983). Development and validation of geriatric depression screening scale: A preliminary report. Journal of Psychiatric Research, 80(1), 37–49. http://doi.org/10.2307/1957152

Zelazo, P. D., & Carlson, S. M. (2012). Hot and cool executive function in childhood and adolescence: Development and plasticity. *Child Development Perspectives, 6*(4), 354–360.

Zonneveld, H. I., Pruim, R. H., Bos, D., Vrooman, H. A., Muetzel, R. L., Hofman, A., … Vernooij, M. W. (2019). Patterns of functional connectivity in an aging population: The Rotterdam Study. *NeuroImage*, *189*(January), 432–444. https://doi.org/10.1016/j.neuroimage.2019.01.041

Supplemental Material

Supplementary Figure 1

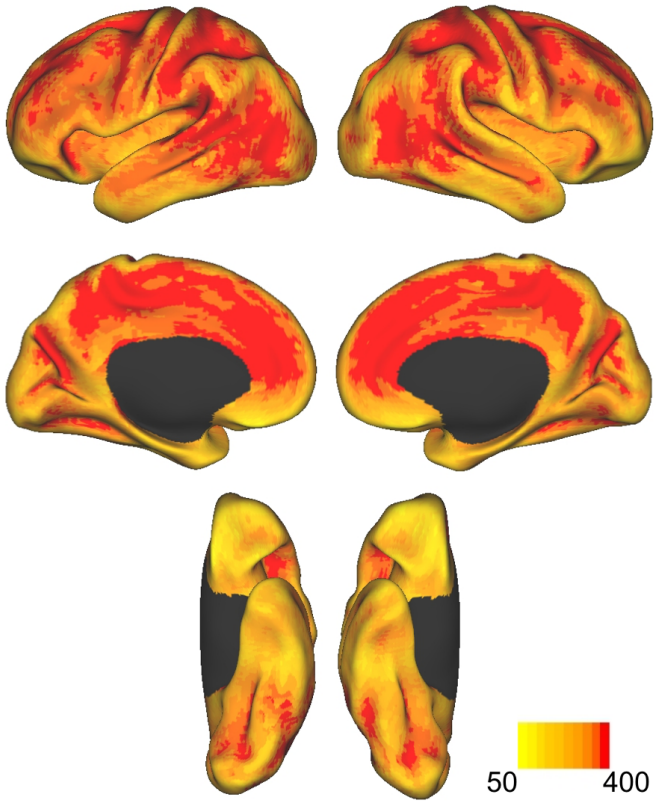

Supplementary Figure 1 Caption: Temporal Signal to Noise. A temporal signal to noise ratio (tSNR) map was created for both runs of each participant's denoised data and averaged. The average group map (N=301) was projected onto an inflated surface, separated by L and R hemispheres. Maps were thresholded to demonstrate that the low end of tSNR values were well above 50. A maximum tSNR of 400 is shown here for visualization purposes.

Supplementary Figure 2

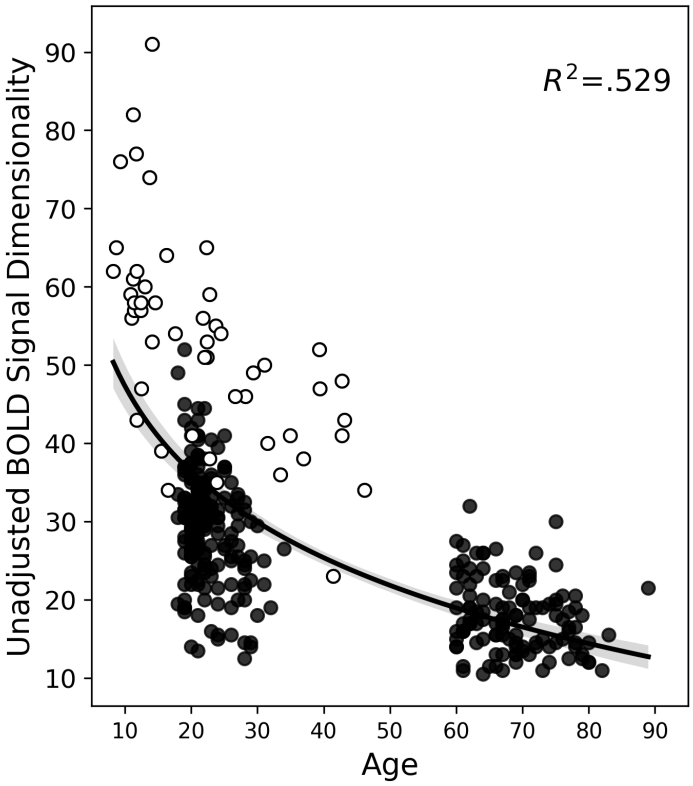

Supplementary Figure 2 Caption: BOLD signal dimensionality. The scatter plot shows BOLD signal dimensionality by age with a power distribution and 95% confidence intervals overlaid. Points in white were contributed by Kundu and colleagues (2018). Here, BOLD dimensionality is not adjusted by number of time points acquired. BOLD dimensionality was averaged across two runs for points in black.

Supplementary Figure 3

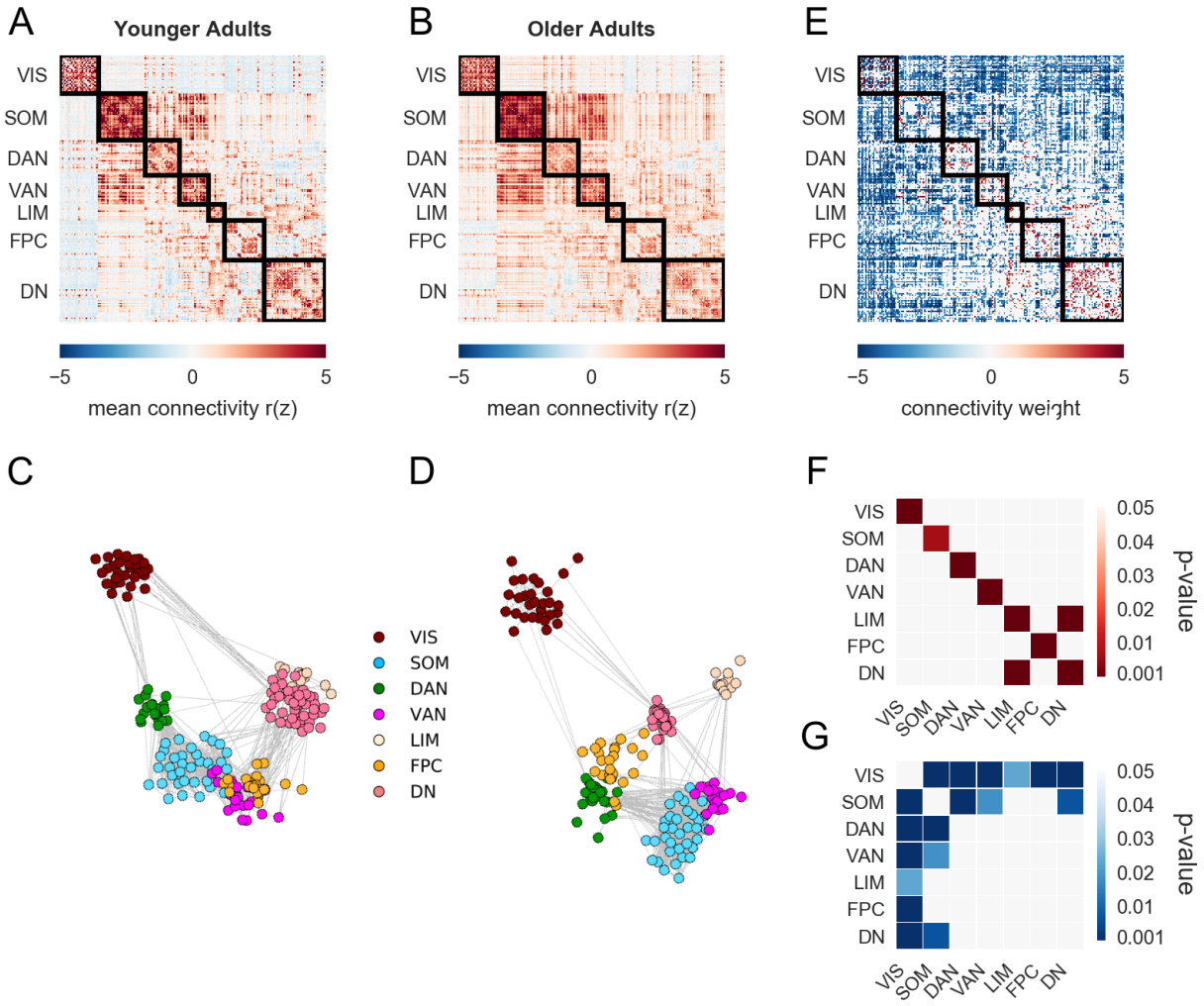

Supplementary Figure 3 Caption: Functional connectomics in younger and older adults. Mean RSFC for the 200-parcellated MEFC data in (A) younger and (B) older adults. Spring-embedded plots with a 7-network solution (5% edge density) of the mean correlation matrices for (C) younger and (D) older adults. (E) Multivariate PLS analysis was used to identify age-related differences in RSFC between younger and older adults. Red color indicates greater RSFC in younger adults, and blue color indicates greater RSFC in older adults. (F-G) Network contributions reflecting differences in large-scale distributed networks. (F) Greater within- and between- network connectivity in young, lower in older adults. (G) Greater within- and between- network connectivity in older adults, lower in younger adults. The mean positive (F) and negative (G) bootstrap ratios within and between networks are expressed as a p-value for each z-score relative to a permuted null model. Higher values indicate greater connectivity than predicted by the null distribution. VIS = visual, SOM= somatomotor, DAN= dorsal attention, VAN = ventral attention, LIM = limbic, FPC= frontoparietal, DN= default.

Supplementary Figure 4

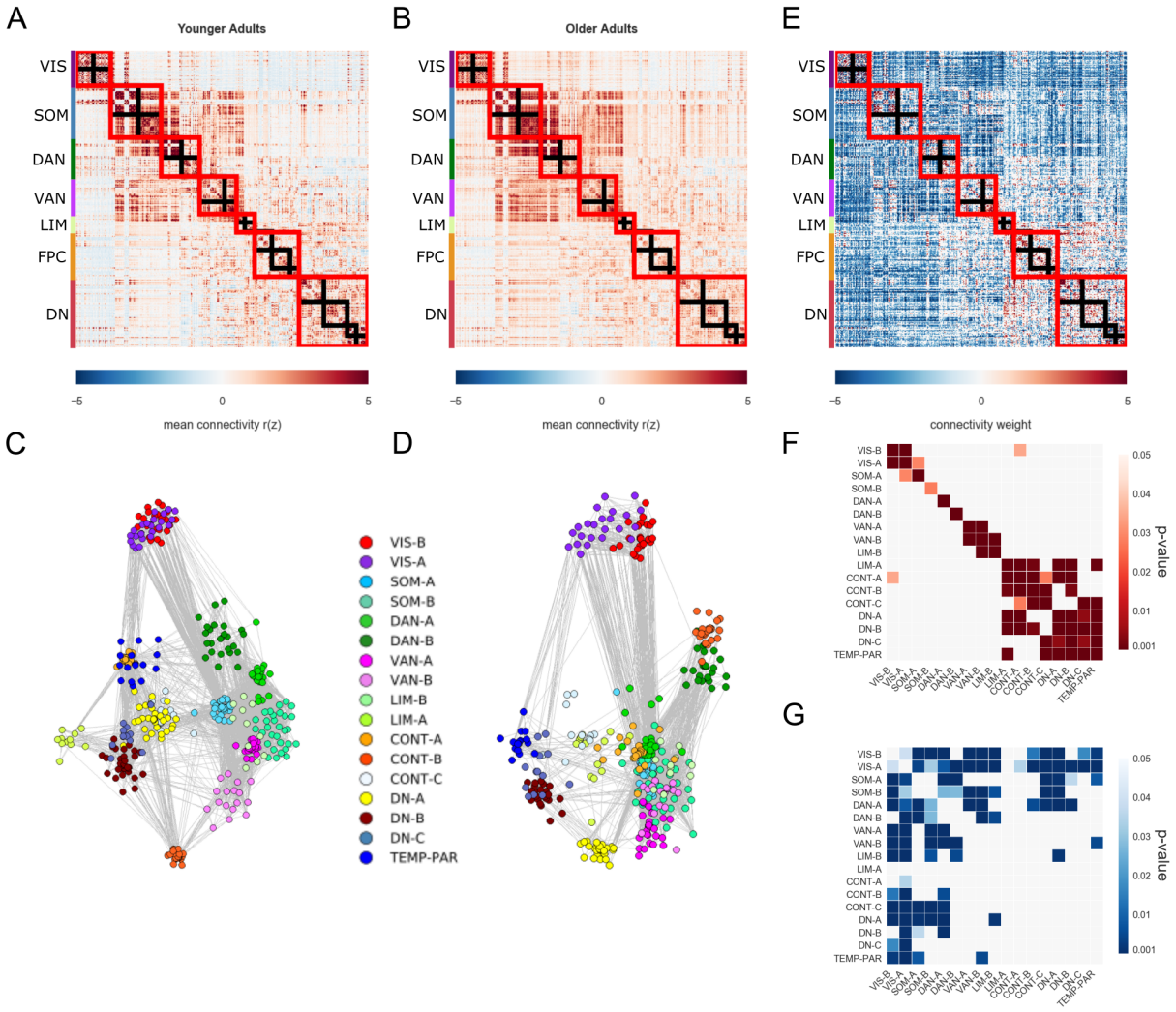

Supplementary Figure 4 Caption: Functional connectomics in younger and older adults. Mean RSFC for the 400-parcellated MEFC data in (A) younger and (B) older adults. Spring-embedded plots with a 17-network solution (5% edge density) of the mean correlation matrices for (C) younger and (D) older adults. (E) Multivariate PLS analysis was used to identify age-related differences in RSFC between younger and older adults. Red color indicates greater RSFC in younger adults, and blue color indicates greater RSFC in older adults ($p<0.0001$; 100% variance explained). (F-G) Network contributions reflecting differences in large-scale distributed networks. (F) Greater within- and between- network connectivity in young, lower in older adults. (G) Greater within- and between-network connectivity in older adults, lower in younger adults. The mean positive (F) and negative (G) bootstrap ratios within and between networks are expressed as a p-value for each z-score relative to a permuted null model. Higher values indicate greater connectivity than predicted by the null distribution. VIS = visual, SOM= somatomotor, DAN= dorsal attention, VAN = ventral attention, LIM = limbic, FPC= frontoparietal, DN= default.

Supplementary Figure 5

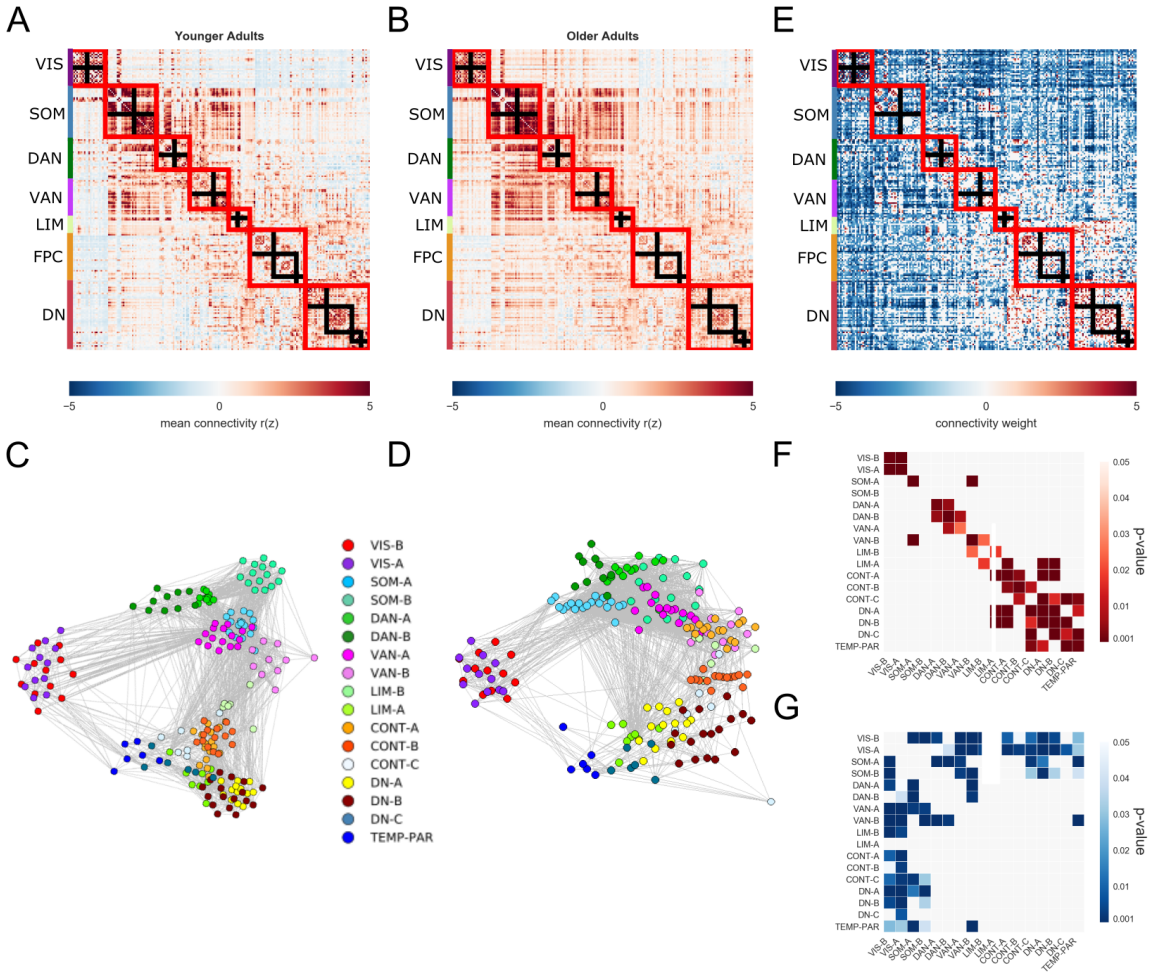

Supplementary Figure 5 Caption: Functional connectomics in younger and older adults. Mean RSFC for the 200-parcellated MEFC data in (A) younger and (B) older adults. Spring-embedded plots with a 17-network solution (10% edge density) of the mean correlation matrices of (C) younger and (D) older adults. The threshold used for the spring-embedded plots was set at a higher threshold due to the sparsity of the graph at thresholds lower than 10%. (E) Multivariate PLS analysis was used to identify age-related differences in RSFC between younger and older adults ($p<0.0001$; 100% variance explained). Red color indicates greater RSFC in younger adults, and blue color indicates greater RSFC in older adults. Network contributions reflecting differences in large-scale distributed networks between (F) younger and (G) older adults. The mean positive bootstrap ratios within and between networks are expresses as a z-score relative to a permuted null model. Higher values indicate greater than expected connectivity in both age groups. VIS = visual; SOM=somatomotor; DAN= dorsal attention; VAN = ventral attention; LIM = limbic, FPC= frontoparietal, DN= default.

Supplementary Figure 6

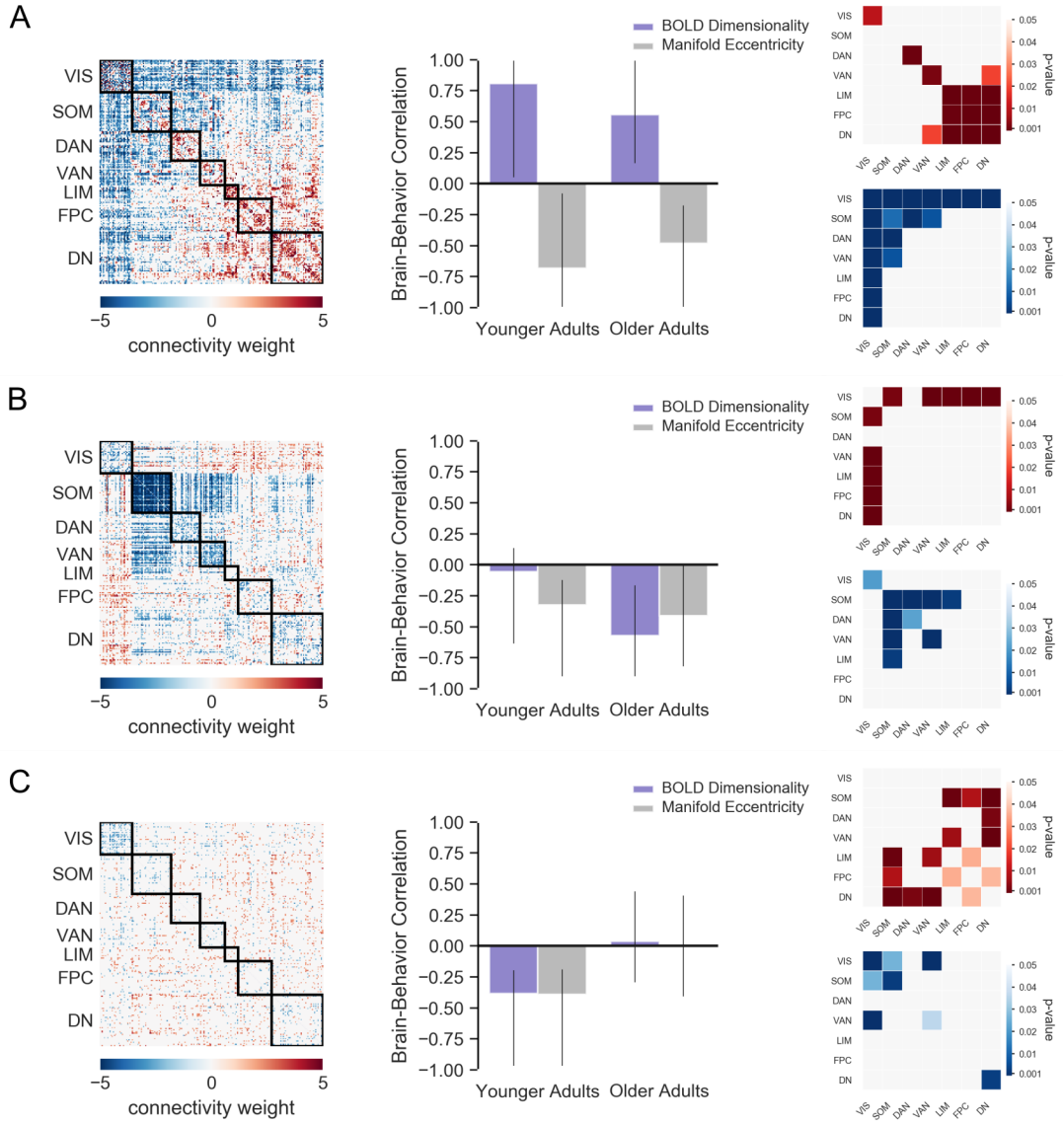

Supplementary Figure 6 Caption: BOLD dimensionality and manifold eccentricity show converging and diverging patterns of RSFC at the 200-parcel resolution. Behavioral PLS analysis identified three patterns of RSFC related to BOLD dimensionality and manifold eccentricity across groups. (A) Shared pattern of connectivity differentiating BOLD dimensionality and manifold eccentricity across age groups ($p < 0.0001$; 53.40% variance explained). (B) Overlap between BOLD dimensionality and manifold eccentricity in older adults as well as manifold eccentricity in younger adults ($p < 0.0001$; 27.99% variance explained). (C) Shared variance for BOLD dimensionality and manifold eccentricity in younger adults ($p = 0.001$; 4.19% variance explained). VIS = visual, SOM= somatomotor, DAN= dorsal attention, VAN = ventral attention, LIM = limbic, FPC= frontoparietal, DN= default.

Supplementary Figure 7

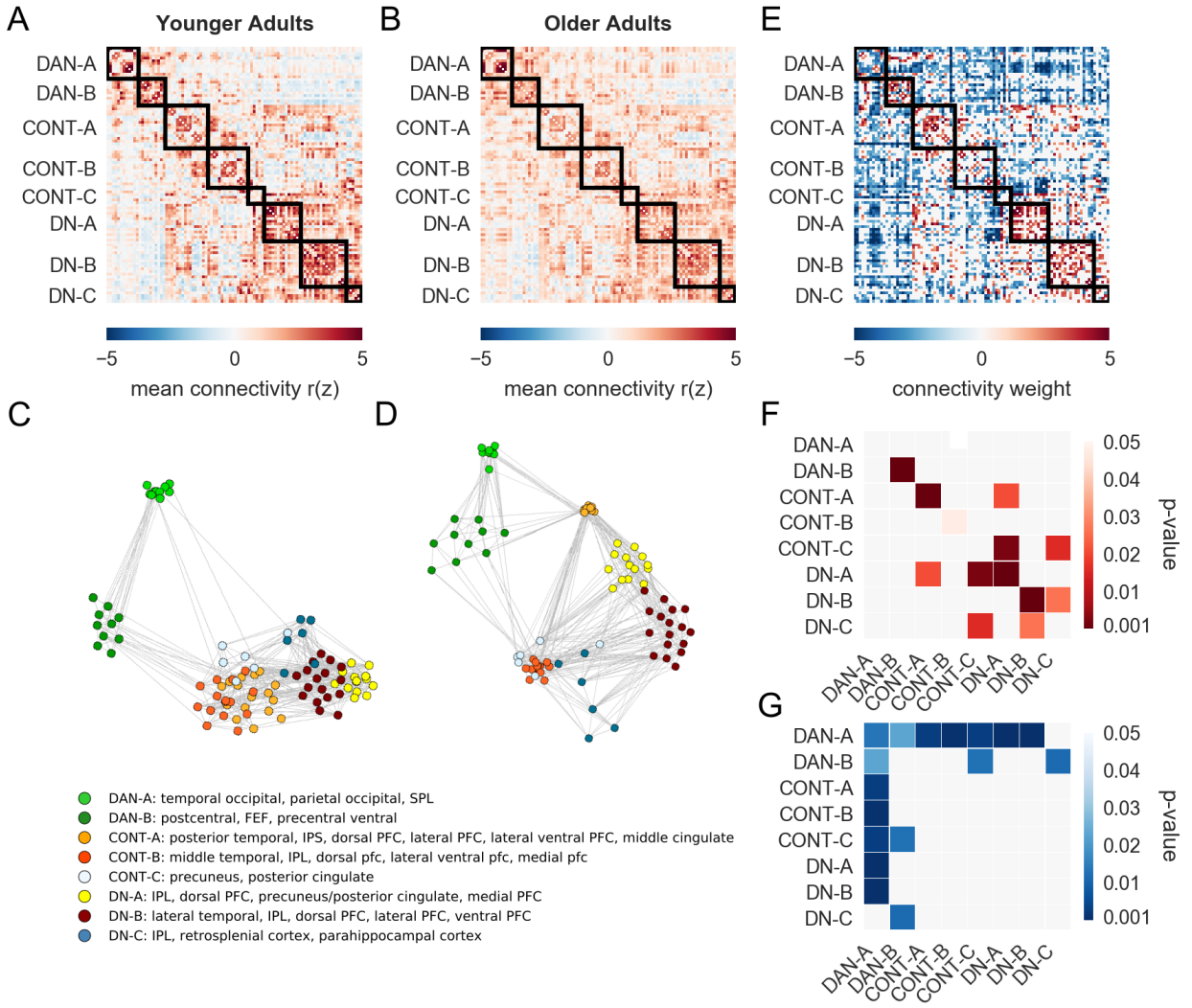

Supplementary Figure 7 Caption: Functional connectivity of the dorsal attention (DAN), frontoparietal control (CONT), and default (DN) sub-networks following Yeo 17-network solution. Mean group connectivity for the 200-parcellated MEFC data in (A) younger and (B) older adults. Spring-embedded plots (10% edge density) of the mean correlation matrices for (C) younger and (D) older adults. A lower threshold was used for the spring-embedded plots due to the sparsity of the graph at higher thresholds ($p<0.0001$;100% variance explained). (E) Differences in RSFC between younger and older adults among DAN, CONT, and DN. (F) Greater within- and between- network connectivity in young. (G) Greater within- and between- network connectivity in older adults.

Supplementary Figure 8

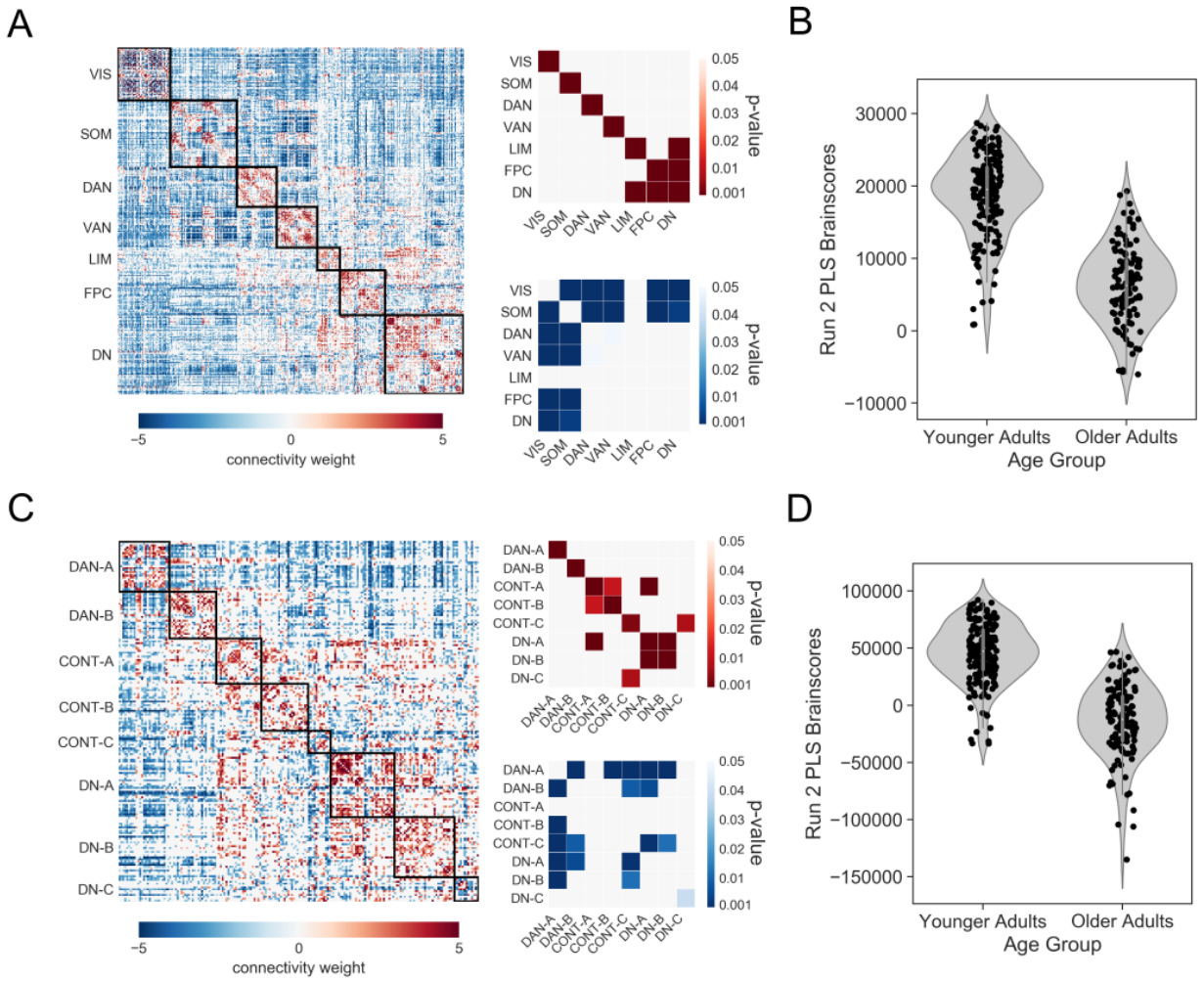

Supplementary Figure 8 Caption: Cross-validation of the PLS results. A) Age differences in the full functional connectome from Run 1. B) Group differences in brain scores computed from Run 2, based upon the edge-weights determined in Run 1. C) Age differences in the functional connectivity of the dorsal attention (DAN), frontoparietal control (CONT), and default (DN) sub-networks from run 1. D) Group differences in brain scores computed from Run 2, based upon the edge-weights determined in Run 1.